ISAS - INTERNATIONAL SCHOOL
FOR ADVANCED STUDIES

Description of the Magnetic Field Lines of a Confined Plasma

Thesis submitted for the degree of

"Doctor Philosophiæ"

CANDIDATE

Norma Reggiani

SUPERVISOR

Prof. Giorgio Turchetti

October 1992

TRIESTE

SISSA - SCUOLA
INTERNAZIONALE
SUPERIORE
DI STUDI AVANZATI
TRIESTE
Strada Costiera 11

Description of the Magnetic Field Lines of a Confined Plasma

Thesis submitted for the degree of

"Doctor Philosophiæ"

CANDIDATE

Norma Reggiani

SUPERVISOR

Prof. Giorgio Turchetti

October 1992

Ao Marcelo.

(Esteja sempre por perto.)

I wish to thank all those who made it possible for me to conclude this Ph.D. work. I am very grateful to

Prof. G. Turchetti, for the support, physical advices, attention and availability during all the process of the development of this thesis;

Prof. P. Londrillo, with whom the MHD code presented in this thesis was developed. He patiently explained many features of this code and I learned a lot of numerical calculations with him;

Prof. I.L. Caldas, for the support, advices and encouragement during all this period;

Monica Malavasi, for the usefull physical discussions and interesting conversations;

all the friends, that made the atmosphere pleasant, particularly (in alphabetical order): Andrea Ferrante, Armando Bazzani, Graziano Servizi, Hilda Cerdeira, Marcelo Alves (for him I thank also the glad hospitality), Marco A.C. Kneipp, Marcos Bordin and Valéria Bevilácqua;

SISSA (International School for Advanced Studies, Trieste - Italy) for offering me very good conditions to develope my work. In particular I would like to thank the attention of Prof. C. Reina;

UNICAMP (Universidade Estadual de Campinas - Brasil) for letting me use its installations to write this thesis. I am grateful in particular to Prof. P. H. Sakanaka, for his availability;

CNPq (Conselho Nacional de Desenvolvimento Científico e Tecnológico - Brasil) for financially supporting my Ph.D. studies in Italy in a very satisfactory way.

Contents

Chapter 1

Introduction

More than one kind of device of plasma confinement has been constructed in order to study the plasma dynamics and to achieve a controlled fusion reactor. Some important problems remain unsolved. One of them is to understand the transport processes which lead to the loss of the plasma confinement. Another is to know how the magnetic fields that confine the plasma evolve in time. These fields have modes that appear and interact with each other. The dynamics of these interactions is nor yet clear.

In this thesis we describe the magnetic fields using two different mathematical tools. One of them describes the magnetic fields by a set of Generalized Standard Maps. Another is a three-dimensional magnetohydrodynamics (MHD) code that gives their time evolution. In both cases we considered a "Reversed Field Pinch" (RFP) configuration of plasma confinement.

In chapter 2 we present the first approach. In a RFP machine, the equilibrium magnetic field lines are reasonably well described by the Taylor theory of the relaxed states [1]. But in the experiences, the observed profiles differ from the equilibrium one and to account for this, some perturbation have to be added to the equilibrium state. The perturbed magnetic field lines can be treated by hamiltonian methods that lead to a description of them by a set of Generalized Standard Maps [2]. These maps differ from the Standard Map for having a perturbative spectrum with more than one mode. Some known features of the Standard Maps are also validy for the Generalized Standard Map and

will be used to study the magnetic field lines.

The diffusion of the magnetic field lines corresponds to the diffusion of the orbits of the Generalized Standard Map. We calculated the diffusion coefficient in the quasi-linear approximation for these maps with different perturbative spectra and we found that the value of this coefficient strongly depends on the number of modes of the spectrum but depends very little on the kind of function appearing as the coefficient of the modes. The KAM curves that exist in these maps act as barriers to the diffusion and it is relevant to study if the break-up of the last of these curves also depends on the perturbative spectra. We used the Newton and Greene methods to find the last KAM curve and then calculated the Lyapunov exponent, the correlation dimension and the residue of this curve for several values of the perturbative parameter ϵ. We found that the necessary value of ϵ to break-up the last KAM curve of these maps (called critical perturbation parameter) depends on the spectrum. The dependence on the number of modes is more accentuated than on the kind of functions that are the coefficients of the modes. We found also a scaling law between the critical perturbation parameter and the number of modes.

In chapter 3 we present the three-dimensional, viscous, resistive MHD code. With this code we describe the time evolution of the magnetic field lines in a cylindrical geometry. We checked this code with an Alfvén wave, which analytical solution we know. Then we evolve in time a magnetic profile without supplying the system with energy. We observed that the field lines are damped and that the reversal of the component B_z is lost.

Finally, in chapter 4 we propose a mechanism that takes into account the effect of the perturbative magnetic spectrum on the time evolution of the magnetic field lines. This mechanism is based on a paper of Gurevich et al [3], in which the transport coefficients are written in terms of the correlation function of the magnetic perturbations.

We tried to be in each chapter the most self-consistent as possible. Therefore, at the beginning of each chapter there is an introduction concerning that chapter, where we also present how it is organized. So, for more detailed introductions, we refer the reader to these sections. In order to make the reading fluent, some topics were discussed in the appendices.

Chapter 2

Description of the Magnetic Field Lines by a Generalized Standard Map

2.1 Introduction

The Taylor theory of relaxed states can be used to describe the magnetic field lines of a "Reversed Field Pinch" (RFP) plasma confinement configuration. This theory is presented in section (2.2.1). In this theory the plasma achieves a state of minimum energy in a process that keeps the helicity constant. This state of minimum energy is an equilibrium configuration of the magnetic field lines.

In real experiments we do not have exactly this equilibrium configuration and to account for this fact some perturbation has to be added to the field lines equations. The field lines are distorced by the perturbation. Indeed, while in the ideal case their intersections with a surface (Poincaré section) are distributed on invariant circles, in presence of the perturbation they belong to invariant sets which can be diffeomorphic to a circle (KAM curve), or to a sequence of circles (islands) or be very scattered in stochastic regions.

The perturbed field lines can be treated by hamiltonian methods and this treatment leads to the description of these lines by a set of Generalized Standard Maps, that differ from the Standard Maps for

having a perturbative spectrum with more than one mode. This perturbative spectrum is determined by experimental observations. The hamiltonian treatment is presented in section (2.2.2) and its application to the RFP configuration in the section (2.2.3).

The existence of KAM curves despite a small perturbation is crucial for the stability analysis. They are real topological barriers to the diffusion, and it is relevant to determine the critical value ϵ_c of the perturbative parameter for which the last KAM curve disappears and diffusion throughout the phase space can occur. When the perturbation is much larger than the critical value, the diffusion can be described by the quasi-linear approximation. We computed the quasi-linear diffusion coefficient of the Generalized Standard Map for different kinds of perturbative spectra. We found that the value of this coefficient depends on the number of modes of the spectrum considered, much more than on the kind of the function appearing as coefficients of the modes. This is presented in the section (2.3).

The critical value gives a lower bound to the validity of the quasi-linear coefficient. In order to analyse if the range of validity of this approximation also depended on the kind of the spectrum, we calculated the critical value of a Generalized Standard Map for different spectra. At a first approach, the orbit with winding number very close to the golden mean was found using the Newton method. The Lyapunov exponent and the correlation dimension of this curve were calculated and we found that the critical value depends on the spectrum. Then we used the Greene method to find the orbits of the convergents of the golden mean. We calculated the Lyapunov exponent and the residue of these orbits. Using the Greene method we could find orbits of a Generalized Standard Map with a broader spectrum than with the Newton method and it was possible to discover a scaling law between the critical value and the number of modes of the spectrum. All this analysis of the break-up of the last KAM curve, also called transition to stochasticity, is presented in section (2.4).

2.2 The Physical Model

2.2.1 Equilibrium State: the Taylor Theory

The toroidal machine, also called toroidal pinch, in principle involves only a toroidal vacuum vessel in which a toroidal magnetic field $\mathbf{B_0}$ is first created by external coils. Then, after creating an initial plasma by a suitable ionizing process, one induces a toroidal current $\mathbf{I}$, which creates a poloidal magnetic field.

There are several remarkable features common to all toroidal pinch experiments:

1) after an initial highly turbulent phase, the plasma sets into a more quiescent state in which the fluctuations are reduced;

2) in this quiescent state the mean magnetic field profiles are essentially independent of the particular experiment or the previous history of the discharge and depend only on a single parameter, the pinch ratio $\Theta = B_\theta(r = a)/ < B_z >$, where $< B_z >$ is an average value of the z-component of the magnetic field, and a is the minor radius of the toroid.

3) if Θ exceeds a certain critical value the quiescent state is one in which the toroidal field is spontaneously reversed in the outer region of the plasma near the vessel wall.

The plasma achieves a quiescent state, that is a minimum-energy state, from a highly turbulent phase through a process known as relaxation.

This process has been theoretically explained by Taylor [1], [4] in his theory of relaxed states, in an amplification of the results of Woltjer [5]. This theory says that in a perfectly conducting plasma, in which the internal energy can be considered negligible compared with the magnetic one, the motion to the relaxed state is constrained by the invariance of the helicity, defined by:

$$K(\alpha, \beta) = \int_V \mathbf{A} \cdot \mathbf{B} \, d^3x \tag{2.1}$$

where the integration is done in an infinitesimal flux tube surrounding a closed line of force and where α, β denote the surfaces delimiting the tube.

These invariants are essentially topological: if one closed line initially links another **n** times then in a perfectly conducting plasma the two loops must remain linked **n** times during any subsequent plasma motion.

The state that minimizes the magnetic energy,

$$W = \frac{1}{2}\int (\nabla \times \mathbf{A})^2 dV \tag{2.2}$$

satisfying the infinity of constrains described above is described by:

$$\nabla \times \mathbf{B} = \lambda(\alpha, \beta)\mathbf{B} \tag{2.3}$$

$$\mathbf{B} \cdot \nabla\lambda = 0 \tag{2.4}$$

But real plasmas are never perfectly conducting. In the presence of resistivity, however small, topological properties of lines of force are no longer preserved. So, flux tubes have no continuous independent existence.

Consequently all topological invariants $K(\alpha, \beta)$ cease to be relevant, not because the magnetic flux changes significantly, but because it is no longer possible to identify the field line to which the flux belongs. However, the sum of all the invariants, that, is the integral of $(\mathbf{A} \cdot \mathbf{B})$ over the total plasma volume V_0, is independent of any topological considerations and of the need of identifying field lines.

To obtain the relaxed state of a slightly resistive turbulent plasma, therefore, it is necessary to minimize the energy subject to the single constraint that the total magnetic helicity

$$K_0 = \int_{V_0} \mathbf{A} \cdot \mathbf{B} dV \tag{2.5}$$

be invariant. Here V_0 is the total volume occupied by the plasma. For a plasma enclosed in a perfectly conducting toroidal shell, the corresponding equilibrium satisfies

$$\nabla \times \mathbf{B} = \mu\mathbf{B} \tag{2.6}$$

where μ is a constant. This parameter μ is directly related to the pinch ratio $\theta = \mu a/2$.

The general solution to the equation (2.6) is

$$\mathbf{B} = \sum_{m,n} \mathbf{B}^{m,n}(r) \tag{2.7}$$

where

$$B_r^{m,n} = \frac{-1}{\sqrt{\nu^2 - n^2}}[nJ'_m(y) + \frac{m\mu}{y}J_m(y)]sin(m\theta + nz) \tag{2.8}$$

$$B_\theta^{m,n} = \frac{1}{\sqrt{\nu^2 - n^2}}[\mu J'_m(y) + \frac{mn}{y}J_m(y)]cos(m\theta + nz) \tag{2.9}$$

$$B_z^{m,n} = J_m(y)cos(m\theta + nz) \tag{2.10}$$

$$y = r\sqrt{\mu^2 - n^2}. \tag{2.11}$$

The term $m = n = 0$ satisfies the boundary condition that the wall is perfectly conducting for any value of μ. The others terms ($m \neq 0, n \neq 0$) satisfy this boundary condition only for discrete values of μ given by

$$n[(\mu^2 - n^2)^{1/2}]J'_m[(\mu^2 - n^2)^{1/2}] + m\mu J_m[(\mu^2 - n^2)^{1/2}] = 0. \tag{2.12}$$

The minimum value of μ that satisfies the equation (2.12) is $\mu = 3.11$, that is, $\Theta = 1.6$. So, for $\Theta < 1.6$, we have only the $m = n = 0$ components, that is, a symmetric state. For $\Theta > 1.6$, for fixed values of Θ there are other components ($m \neq 0, n \neq 0$), together with the component $m = n = 0$.

We used as the equilibrium state of the RFP magnetic field lines the symmetric state, that is called the "Bessel Function Model":

$$B_r = 0 \tag{2.13}$$

$$B_z = B_0 J_0(\mu r/a) \tag{2.14}$$

$$B_\theta = B_0 J_1(\mu r/a) \tag{2.15}$$

According to this model a reversal in the B_z component is predicted to $\Theta > 1.2$. The profiles obtained with these equations fit well with the experimental data, except for the outer region of the torus. A reason for this discrepancy is that μ, which would be uniform in a fully relaxed state, falls off near the wall. This effect has been discussed in detail by Ortolani [6].

2.2.2 Hamiltonian Treatment of the Perturbed States

The equilibrium equations for the magnetic field lines, parametrized by θ, are:

$$\begin{aligned} \frac{dr}{d\theta} &= \frac{rB_r}{B_\theta} = 0 \\ \frac{d\psi}{d\theta} &= \frac{rB_\psi}{RB_\theta} = \frac{rJ_0(\mu r/a)}{RJ_1(\mu r/a)} = \Omega(r) \end{aligned} \tag{2.16}$$

where a and R are the minor and major radii of the toroid respectively.

To describe a realistic situation, it is necessary to introduce an appropriate perturbation in (2.16). This has been done by Turchetti et al [2]. The equations of motion become:

$$\begin{aligned} \frac{dr}{d\theta} &= \epsilon \frac{rB_r^{(1)}(r,\psi;\theta)}{B_\theta(r)} \\ \frac{d\psi}{d\theta} &= \Omega(r) + \epsilon \frac{rB_\psi^{(1)}(r,\psi;\theta)}{RB_\theta(r)} \end{aligned} \tag{2.17}$$

The deformations of the perturbed magnetic field lines can be studied with the methods borrowed from hamiltonian mechanics [7]. The equations of motion leave invariant the measure

$$W_2 = RB_\theta(r) dr \wedge d\psi. \tag{2.18}$$

The differential form

$$dH = (RB_\theta\Omega + \epsilon r B_\psi^{(1)})dr - \epsilon r R B_r^{(1)} d\psi \tag{2.19}$$

is exact and

$$H = H(\rho, \psi, \theta) \tag{2.20}$$

where

$$\rho = R \int B_\theta(r) dr. \tag{2.21}$$

The equations of motion can be written as

$$\frac{d\rho}{d\theta} = -\frac{\partial H}{\partial \psi} \tag{2.22}$$

$$\frac{d\psi}{d\theta} = \frac{\partial H}{\partial \rho} \tag{2.23}$$

and preserve the ordinary Lebesgue measure

$$w = d\rho \wedge d\psi \tag{2.24}$$

In the RFP model considered by Turchetti et al [2] only the first order terms were taken in the Bessel function power series expansion in the measure and in the equations of motion. So, the measure takes the form:

$$W_2 = R\frac{\mu B_0}{2} r dr \wedge d\psi = R\frac{\mu B_0}{4} d\rho \wedge d\psi \tag{2.25}$$

where

$$\rho = r^2 \tag{2.26}$$

The presence of a constant factor in the measure is only a matter of notational convenience.

The hamiltonian (2.20) can be written as

$$H(\rho, \psi, \theta) = H^{(0)}(\rho) + \epsilon H^{(1)}(\rho, \psi, \theta). \tag{2.27}$$

The equations of motion are:

$$\begin{aligned} \frac{d\rho}{d\theta} &= -\epsilon\frac{\partial H^{(1)}}{\partial\psi} \equiv -\epsilon f(\rho,\psi,\theta) \\ \frac{d\psi}{d\theta} &= \frac{\partial H^{(0)}}{\partial\rho} + \epsilon\frac{\partial H^{(1)}}{\partial\rho} \equiv \Omega(\rho) + \epsilon g(\rho,\psi,\theta) \end{aligned} \tag{2.28}$$

where $\Omega(\rho) = \Omega(r) = \Omega(\sqrt{\rho})$, $f = \frac{\sqrt{\rho}B_r^{(1)}}{B_\theta(r)}$ and $g = \frac{\sqrt{\rho}B_\phi^{(1)}}{RB_\theta(r)}$.

The Taylor's expansions in ϵ of ρ and ψ are given by

$$\rho(\theta) = \rho^{(0)}(\theta) + \sum_{k\geq 1}\epsilon^k\rho^{(k)}(\theta) \tag{2.29}$$

$$\psi(\theta) = \psi^{(0)}(\theta) + \sum_{k\geq 1}\epsilon^k\psi^{(k)}(\theta) \tag{2.30}$$

where $\rho(0) = \rho^{(0)}(0)$ and $\psi(0) = \psi^{(0)}(0)$.

At zero order the equations (2.28) read

$$\begin{aligned} \frac{d\rho^{(0)}}{d\theta} &= 0 \\ \frac{d\psi^{(0)}}{d\theta} &= \Omega(\rho) \end{aligned} \tag{2.31}$$

and their solutions are

$$\begin{aligned} \rho^{(0)}(\theta) &= \rho(0) \\ \psi^{(0)}(\theta) &= \psi(0) + \theta\Omega(\rho(0)). \end{aligned} \tag{2.32}$$

At first order the equations take the form

$$\begin{aligned} \frac{d\rho^{(1)}}{d\theta} &= -\epsilon f(\rho^{(0)},\psi^{(0)}(\theta),\theta) \\ \frac{d\psi^{(1)}}{d\theta} &= \Omega'(\rho^{(0)})\rho^{(1)}(\theta) + \epsilon g(\rho^{(0)},\psi^{(0)}(\theta),\theta) \end{aligned} \tag{2.33}$$

and the solutions to these equations are

$$\begin{aligned} \rho(\theta) &= \rho^{(0)} + \epsilon\int_0^\theta dt f(\rho^{(0)},\psi^{(0)}(t),t) \\ \psi(\theta) &= \psi^{(0)} + \theta\Omega(\rho^{(0)}) + \epsilon\Omega'(\rho^{(0)})\int_0^\theta dt\int_0^t ds f(\rho^{(0)},\psi^{(0)}(s),s) \\ &\quad + \epsilon\int_0^\theta dt g(\rho^{(0)},\psi^{(0)}(t),t) \end{aligned} \tag{2.34}$$

where we have written $\rho(0) \equiv \rho^{(0)}$ and $\psi(0) \equiv \psi^{(0)}$. So, the Poincaré section at $\theta = 2\pi$ of the flow (2.34) reads

$$M : \begin{cases} \rho_{k+1} &= \rho_k + \epsilon F(\rho_k, \psi_k) \\ \psi_{k+1} &= \psi_k + \omega(\rho_k) + \epsilon G(\rho_k, \psi_k) \end{cases} \tag{2.35}$$

where $\omega(\rho) = 2\pi\Omega(\rho) = 2\pi\Omega(r)$.

This map is area-preserving at first order

$$\frac{\partial(\rho_{k+1}, \psi_{k+1})}{\partial(\rho_k, \psi_k)} = 1 + O(\epsilon^2). \tag{2.36}$$

One can observe that F and G satisfy

$$\frac{\partial F}{\partial \rho} + \frac{\partial G}{\partial \psi} - \omega' \frac{\partial F}{\partial \psi} = 0 \tag{2.37}$$

where $\omega' \equiv \frac{d\omega}{d\rho} = \frac{2\pi}{2r}\frac{d\Omega}{dr}$. Equation (2.37) allows one to introduce a generating function

$$g(\rho_{k+1}, \psi_k) = g_0(\rho_{k+1}, \psi_k) + \epsilon g_1(\rho_{k+1}, \psi_k) \tag{2.38}$$

which produces an exactly area preserving map, M_{sym}, which agrees with (2.35) up to order ϵ^2, that is M_{sym}=M+O(ϵ^2). This new map reads [2],

$$M : \begin{cases} \rho_{k+1} &= \rho_k + \epsilon F(\rho_{k+1}, \psi_k) \\ \psi_{k+1} &= \psi_k + \omega(\rho_{k+1}) + \epsilon[G(\rho_{k+1}, \psi_k) - \omega'(\rho_{k+1}) F(\rho_{k+1}, \psi_k)] \end{cases} \tag{2.39}$$

This map is defined in an implicit way, but it is easily inverted, whenever the inverse exists, using an iterative procedure.

A further approximation can be done which consists in neglecting in the sympletic map the perturbation in the angular component and approximating the perturbation in the radial component with a piecewise constant function namely

$$\begin{aligned} F(\rho_{k+1}, \psi_k) &= \textstyle\sum_{j=1}^{N} F(r^2_{k+1,j}, \psi_k)\Theta_j(\rho_{k+1}) \\ r_{k+1,j} &= a(\frac{2j-1}{2N}) \end{aligned} \tag{2.40}$$

where $\Theta_j(\rho_{k+1}) = 1$ for $\rho_{k+1} \in I_j \equiv [(a(j-1)/N)^2, (aj/N)^2]$ and $\Theta_j(\rho_{k+1}) = 0$ anywhere else for j=1,...,N. If we replace ρ_{k+1} with ρ_k the error in the radial part with respect to the exact map is still of order ϵ^2, but the advantage is obvious: one has an explicit locally (in any interval I_j) sympletic map. In this way, the exact map has been replaced by a set of N Sectorial Generalized Standard Maps M_j defined in the intervals I_j where

$$M_j : \begin{cases} \rho_{k+1} &= \rho_k + \epsilon F(r_{k,j}^2, \psi_k) \\ \psi_{k+1} &= \psi_k + \omega(\rho_{k+1}) \end{cases} \tag{2.41}$$

2.2.3 The RFP Magnetic Field Lines

The perturbation of the magnetic field lines is considered stationary and its poloidal component null. The stationary condition is physically well justified since the discharge time is much longer than the relaxation time. The second assumption is made mainly for simplicity. The perturbation considered satisfies $\nabla \cdot \mathbf{B} = 0$, so that the choice of $B_r^{(1)}$ determines $B_\psi^{(1)}$ and vice-versa.

The radial component is described by

$$B_r^{(1)} = f(r)\frac{\partial P}{\partial \psi}(\psi, \theta) \tag{2.42}$$

where f(r) is a continuous function in r which vanishes on the major axis and on the toroidal shell,

$$f(r) = B_0 \frac{r(a-r)}{a^2}, \tag{2.43}$$

and $P(\psi, \theta)$ is a trigonometric polynomial which takes into account the experimental observed spectra and is given by

$$P(\psi, \theta) = (b_0 + b_1 sin\theta)[\sum_n \frac{a_n}{n} cos(n\psi)]. \tag{2.44}$$

The divergence free condition for the perturbed part of the magnetic field $B^{(1)}(r, \psi, \theta)$ in cylindrical coordinates reads:

$$\frac{1}{r}\frac{\partial}{\partial r} r B_r^{(1)} + \frac{1}{R}\frac{\partial}{\partial \psi} B_\psi^{(1)} = 0 \tag{2.45}$$

and using (2.42), the toroidal component is given by

$$B_{\psi}^{(1)} = R\left(\frac{f(r)}{r} + f'(r)\right) P(\psi,\theta) \tag{2.46}$$

So, the field components $B^{(1)}$ can be written

$$B_{r}^{(1)} = B_0 \frac{r(a-r)}{a^2}(b_0 + b_1 sin\theta)\sum_n a_n \sin(n\psi) \tag{2.47}$$

$$B_{\psi}^{(1)} = -B_0 R\frac{(2a-3r)}{a^2}(b_0 + b_1 sin\theta)\sum_n \frac{a_n}{n}\cos(n\psi) \tag{2.48}$$

A further simplification is made using the power series expansion, truncated at the first order, of the Bessel functions $J_0(\mu r/a)$, $J_1(\mu r/a)$, so that

$$B_{\theta}(r) = B_0 \frac{\mu}{2} r \tag{2.49}$$

$$\Omega(r) = \frac{raJ_0(\mu r/a)}{RJ_1(\mu r/a)} = \frac{2a}{\mu R}\left(1 - \frac{r^2}{r_*^2}\right) \tag{2.50}$$

where r_* is the zero of the Bessel function $J_0(\mu r/a)$, $r_* = (2.4/\mu)a$.

Using the expressions of the the magnetic field components, $B_r^{(1)}$ and $B_{\psi}^{(1)}$, in the perturbed equations of the field lines (2.17), changing from the variable r to ρ and using equations (2.49) and (2.50), we have to the magnetic field lines:

$$\begin{aligned} \frac{d\rho}{d\theta} &= \frac{2\epsilon}{\mu}\frac{\rho^{1/2}(a-\rho^{1/2})}{a^2}(b_0 + b_1\sin\theta)\sum_n a_n \sin(n\psi) \\ \frac{d\psi}{d\theta} &= \frac{2}{\mu R}(1 - \frac{\rho}{r_*^2}) + \frac{2\epsilon}{\mu}\frac{(3\rho^{1/2} - 2a)}{a^2}(b_0 + b_1\sin\theta)\times \\ &\qquad \textstyle\sum_n \frac{a_n}{n}\cos(n\psi) \end{aligned} \tag{2.51}$$

With the method described in the previous section we can obtain an exact sympletic map, written in an implicity way:

$$\begin{cases} \rho_{k+1} &= \rho_k + \epsilon' F(\rho_{k+1}, \psi_k) \\ \psi_{k+1} &= \psi_k + \omega(\rho_{k+1}) + \epsilon'(G(\rho_{k+1}, \psi_k) - \omega'(\rho_{k+1}) F(\rho_{k+1}, \psi_k)) \end{cases} \tag{2.52}$$

This map can be substituted by a set of Sectorial Standard Maps as is shown in the former section, given by the equations (2.51). The expressions of $F(\rho, \psi)$ and $G(\rho, \psi)$ and the values of the parameters used can be found in appendix A.

In the figures (2.1) and (2.2) we show the phase portraits for $\epsilon = 10^{-3}$ and $\epsilon = 7 \times 10^{-3}$, respectively, from the section of flow (2.51), obtained with a fourth order Runge-Kutta integration, the exact sympletic implicit map (2.52) and the Sectorial Standard Map approximation. The inversion of (2.52) is obtained recursively with few steps for the considered values of ϵ.

The results show that the lines of force can be studied with the sympletic map or with the Sectorial Standard Map even at values of ϵ for which the stochastic region is one half of the phase space.

One advantage of this kind of approach is the computer time consumption. In CPU time, 3650s are necessary to integrate the flow and do the Poincaré section, while 14.03s and 1.12s are necessary to the exact sympletic map and to the Sectorial Standard Map respectively. So, this last one can provide a good approximation to the exact Poincaré section (obtained from the equation (2.51)) in a very short time.

So, the Generalized Standard Map is a good tool to study the magnetic field lines of a confined plasma in a RFP configuration. Some of its properties are presented in the appendix B. In the next sections we will present studies of the effect of different perturbative spectra on the quasi-linear diffusion coefficients and on the transition to stochasticity of this kind of map. The importance of this analysis for the Generalized Standard Map is to understand how different perturbations will affect the equilibrium magnetic lines. In order to analyse just the dependence of the diffusion coefficient and the transition to stochasticity on the number of modes and on the kind of the coefficients of these modes, we normalized the perturbative spectra, such that we were always comparing systems with the same magnetic energy.

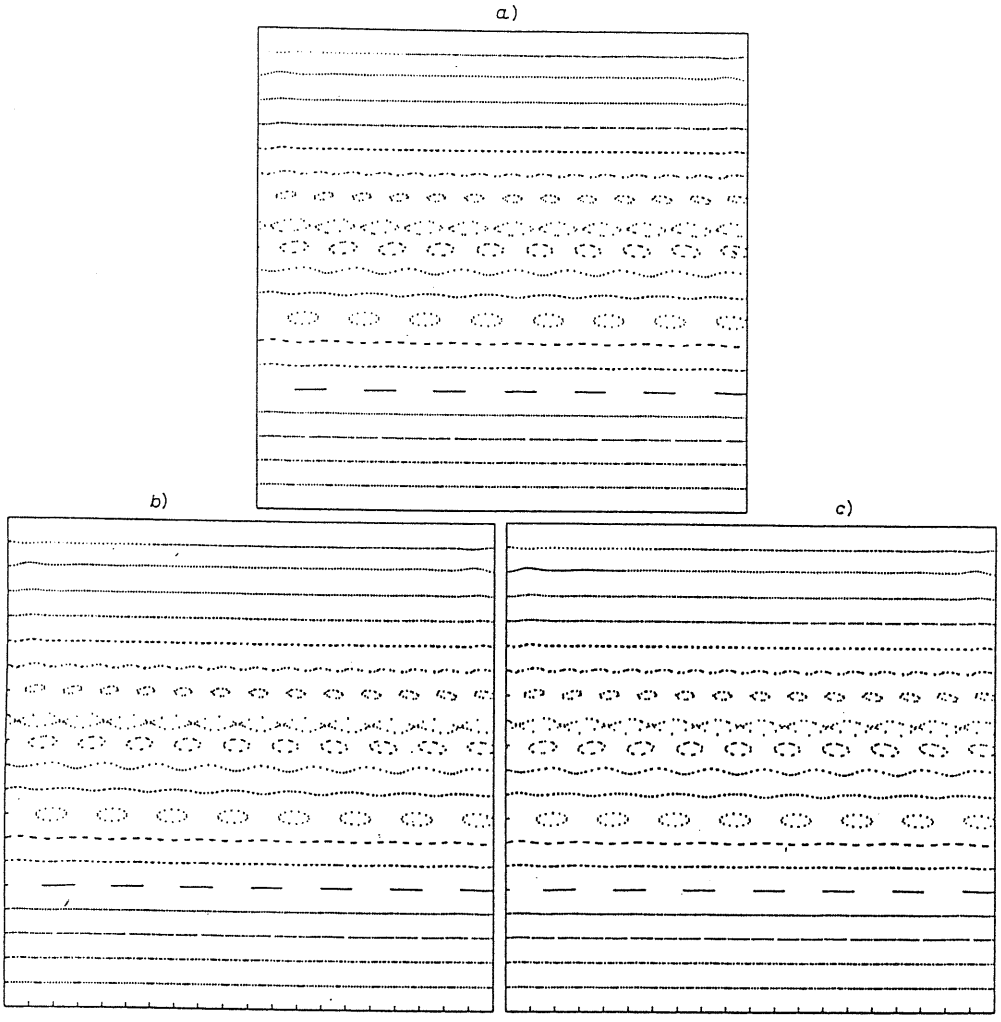

Figure 2.1: Poincaré section of the flow (A), sympletic map (B) and Sectorial Standard Map (C) for $\epsilon = 10^{-3}$. (Figure taken from the reference [2]).

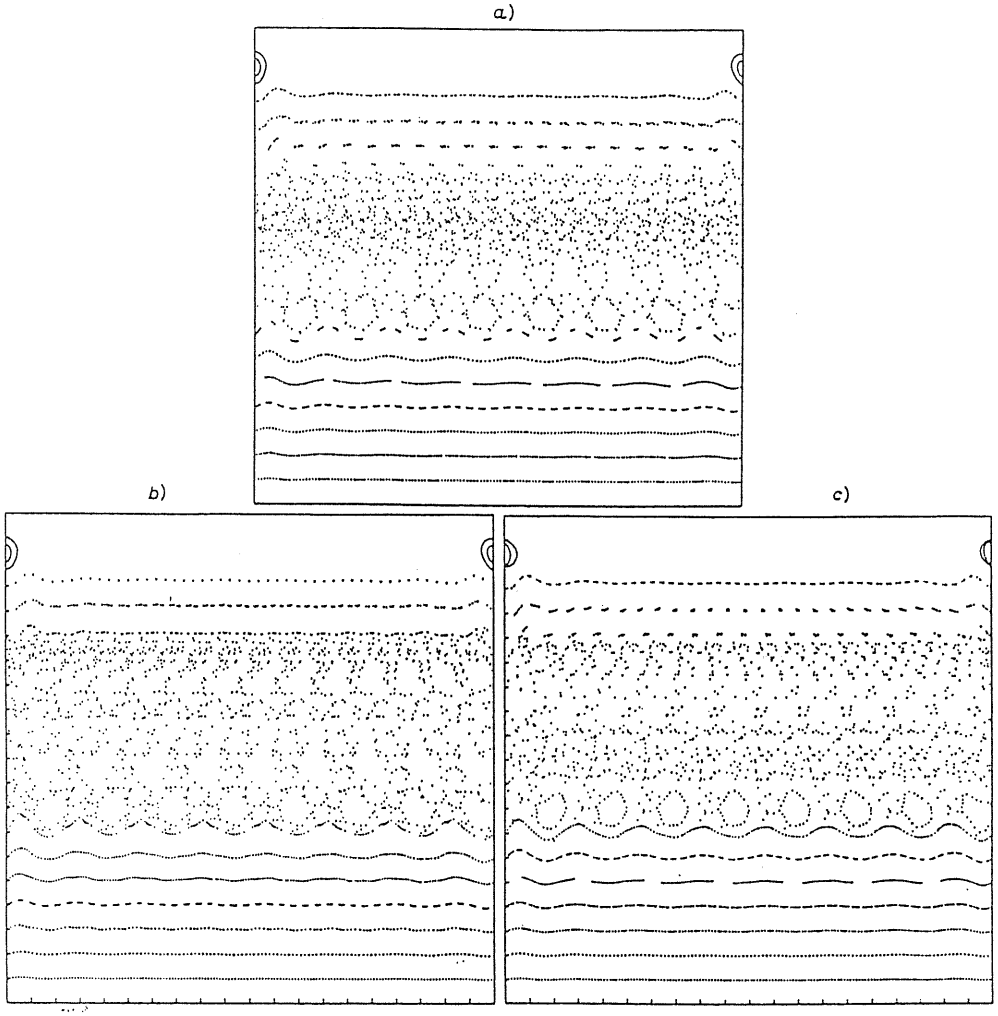

Figure 2.2: Poincaré section of the flow (A), sympletic map (B) and Sectorial Standard Map (C) for $\epsilon = 7 \times 10^{-3}$. (Figure taken from the reference [2]).

2.3 Diffusion Coefficient

In the previuos section we reduced the problem of integrating the equations of the magnetic field lines to the study of a sectorial Generalized Standard Map:

$$M_j : \begin{cases} \rho_{k+1} &= \rho_k + \epsilon F(\rho_{k,j}, \psi_k) \\ \psi_{k+1} &= \psi_k + \omega(\rho_{k+1}) \end{cases} \tag{2.53}$$

where the function $F(\rho_{k,j}, \phi_k)$ is defined in the interval $\rho_j \in [(a(j-1)/N)^2, (aj/N)^2]$ and is given in the appendix A. Then the diffusion of the magnetic field lines in the radial coordinate corresponds to the diffusion in the Generalized Standard Map. The diffusion coefficient is defined by:

$$D = \lim_{k\to\infty} \frac{< (\rho_k - \rho_0)^2 >_{\rho_0,\psi_0}}{2k} \tag{2.54}$$

where $< . >_{\rho_0,\psi_0}$ is an average over an ensemble of initial values (ρ_0, ψ_0). When the orbits are stochastic, the phases ψ_k are uncorrelated over a single map step, and we obtain the quasi-linear approximation for the diffusion coefficient

$$D_{Q.L.} = \frac{1}{2\pi} \int_0^{2\pi} (\Delta\rho_1)^2 d\psi_0. \tag{2.55}$$

We computed the quasi-linear diffusion coefficient of the map (2.53) for different forms of the function $F(\rho_j, \psi)$, that is given by:

$$F(\rho_j, \psi) = \int_0^{2\pi} dt \frac{2}{B_0\mu} B_r^{(1)}(\rho_j, \psi(t), t), \tag{2.56}$$

where $B_r^{(1)}$ is:

$$B_r^{(1)}(\rho, \psi, \theta) = B_0 f(\rho)(b_0 + \sum_{m=1} b_m(m\theta))[\sum_n a_n sin(n\ \psi)]. \tag{2.57}$$

We compared the quasi-linear diffusion coefficient varying the toroidal spectra, keeping fixed the poloidal apectra in agreement with the experimental observation [26]:

$$b_0 = 0.5, b_1 = 1.0, b_2 = 0.25. \tag{2.58}$$

For the toroidal spectra we have taken:

$$a_n = \frac{n}{10} \qquad n = 8, 9, 10 \tag{2.59}$$

whereas for the higher components a_n we considered a linear decay of the spectrum until a n_{max}

$$a_n = \frac{n_{max} - n}{n_{max} - 10} \qquad 11 \leq n \leq n_{max} \tag{2.60}$$

or an exponential decay,

$$a_n = e^{-\alpha(n-10)} \qquad n \geq 11. \tag{2.61}$$

In order to compare the diffusion of the magnetic field lines with different poloidal spectra but with the same magnetic energy, we normalized the map:

$$\mathbf{M_j} : \begin{cases} \rho_{k+1} = & \rho_k + \eta \dfrac{F(\rho_{j,k}, \psi_k)}{||F(\rho_{j,k}, \psi_k)||} \\ \psi_{k+1} = & \psi_k + \omega(\rho_{k+1}) \end{cases} \tag{2.62}$$

where $||.||$ is the usual L^2-norm in the angle variables θ, ψ and

$$\eta = \epsilon ||F(\rho_j, \psi)||. \tag{2.63}$$

The quasi-linear diffusion coefficient in each region $[\rho_{j-1}, \rho_j]$ has the form

$$D(\rho) = \frac{\epsilon^2}{2} f^2(\rho) \sum_{m_1, m_2} b_{m_1} b_{m_2} \sum_{k_1 = k_2} \frac{S_{m_1} S_{m_2} + C_{m_1} C_{m_2}}{(m_1^2 - k_1^2 \Omega^2)(m_2^2 - k_2^2 \Omega^2)}, \tag{2.64}$$

where S_m and C_m are constants only depending on the poloidal and toroidal components of the perturbative spectrum (b_m and a_k, respectively).

In the figure (2.3) we can see the diffusion coefficient versus n_{max} for an exponential and linear decay. Given a certain n_{max}, the constant α of the exponential decay was calculated such that the spectra have the same magnetic energy. The value of η considered was 10^{-2}, because

with this value the orbits were stochastic. We can observe that the diffusion coefficient is almost independent of the kind of decay, depending essencially on the number of modes [26].

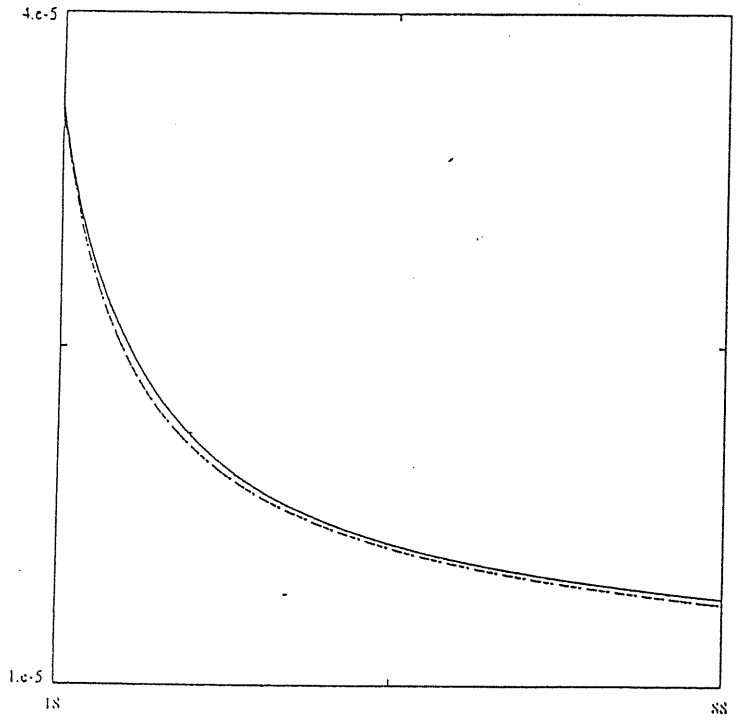

Figure 2.3: diffusion coefficient versus n_{max} for an exponential and a linear decay

2.4 Transition to Stochasticity

The quasi-linear approximation is valid when the orbits are completely stochastic and in this sense the critical parameter gives us a lower

bound to the validity of this approximation. We analized if this range of validity is the same for different spectra, that means to analyse if the transition to stochasticity depends on the perturbative spectra or not.

We are considering critical value the value of the perturbative parameter for which the KAM curve with winding number given by the golden mean is broken. For the Standard Map, this is the last KAM curve that is broken. We assume that this is valid also for the Generalized Standard Map given by:

$$\mathbf{M}: \begin{cases} \rho_{k+1} = & \rho_k + \eta \dfrac{V(\psi_k)}{||V(\psi_k)||} \\ \psi_{k+1} = & \psi_k + \omega(\rho_{k+1}) \end{cases} \quad (2.65)$$

where the perturbative spectrum is normalized. Details about the Generalized Standard Map can be found in appendix B.

In a first analysis [27], we considered two kinds of decay:

$$V(\psi_k) = \sum_{n=1}^{N} \frac{sin(2\pi n\psi_k)}{n}, N = 5, 10 \quad (2.66)$$

$$V(\psi_k) = \sum_{n=1}^{M} sin(2\pi n\psi_k)e^{0.1(1-n)}, M = 5, 10 \quad (2.67)$$

When a KAM curve is broken, it becomes a cantor set [10]. We have analysed this transition calculating the Lyapunov exponent and the correlation dimension of the KAM curve, for various values of perturbation.

In order to calculate the Lyapunov exponent and the correlation dimension of a curve with a certain winding number it is necessary to know the initial conditions of this curve. We have calculated the initial conditions of the KAM curve with winding number given by the golden mean for various values of perturbation parameter numerically, with a Newton method. This could be done because the generalized standard map is a twist map, that is, the winding number is a monotonic increasing function of r. This method, if it will converge, converges within few steps. The value of the winding number is given by a limit that converges as the inverse of the number of iterations of the map. So, in order to have a reasonable precision we must iterate the map

many times. When the value of the perturbation parameter is slightly higher than the critical one, the convergence of the Newton method is really very slow. When it is even higher, the method does not converge, as should be expected, because the curve is already stochastic.

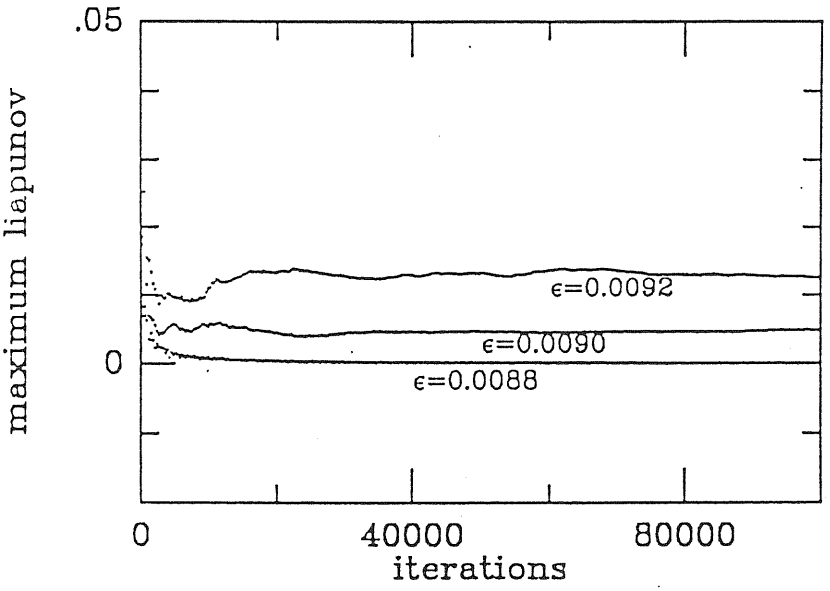

Figure 2.4: value of the Lyapunov exponent for some values of the perturbation, when we consider 10 modes of a spectrum with an exponential decay.

The Lyapunov exponent is defined by [29]:

$$\lambda = \lim_{n\to\infty} \frac{1}{n} log|DT^n(\mathrm{x})| \tag{2.68}$$

where by T^n we mean T composed with itself n times and D denotes differentiation with respect to the two-vector x. When this exponent is null, we have a regular orbit. When it is positive, we observe an exponential separation of nearby orbits and we have a stochastic orbit. So, the Lyapunov exponent of a orbit show us the mean exponential

rate of the divergence of the orbits surrounding it, in other words, if it is regular or not.

In the calculation of this Lyapunov exponent the norm of equation (2.68) increases exponentially with n, and this leads to overflow. In order to avoid this, we used the method of Benettin et al [30] that consists of applying the tangent map on a random vector which is normalized step by step. For values of the perturbative parameter less than the critical one, a good convergence is reached with 100000 iterations, as can be seen in the figure (2.4), where the Lyapunov exponent of the spectrum (2.67) with $N = 10$ is shown for some values of ϵ.

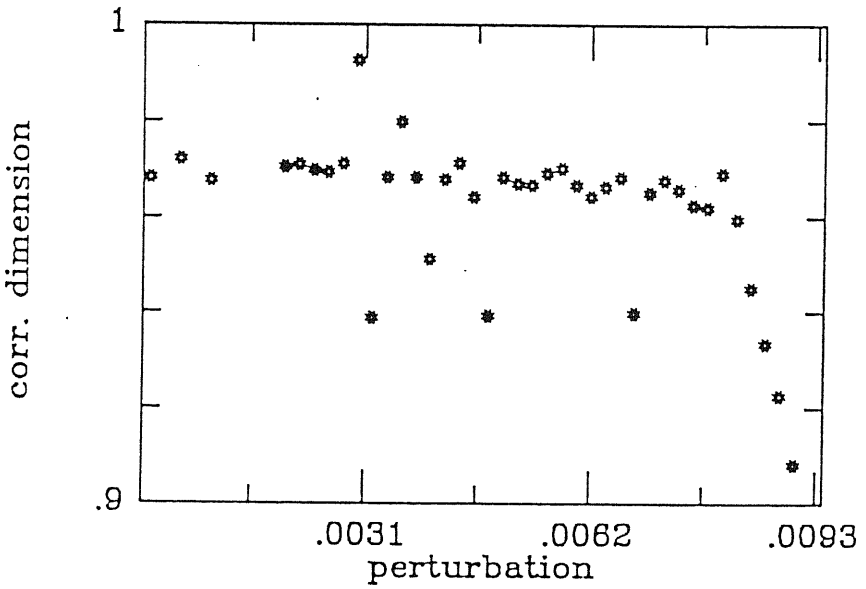

Figure 2.5: value of the correlation function for some values of the perturbation, when we consider 10 modes of a spectrum with an exponential decay.

The correlation dimension is defined as [31]:

$$\nu(\mu) = \lim_{l \to 0} \frac{logC(l;\mu)}{logl}$$

$$C(l;\mu) = \int_{E \times E} \theta(l - \|x - y\|) d\mu(x) d\mu(y)$$

where $|.|$ denotes the usual norm in $\mathbf{R}^n$. E is the invariant limit set and $\mu(x)$ is the measure, that is given by $\mu(x) = \lim_{n\to\infty} \frac{\nu_n(x)}{n}$, where $\nu_n(x)$ is the number of points of the orbit $\{x_0, Tx_0, ..., T^{n-1}x_0\}$, $x_0 \in E$, which belong to the set $x \in E$. So the integral is done considering just the values of x and y covered by the iterations $T^n x_0$ and $T^n y_0$ respectively.

The integral $C(l;\mu)$ gives the number of couples (x, y) such that the distance between them is less than l. When the curve is dense, the limit $\nu(\mu)$ converges to 1. When the perturbation grows and this curve becomes a cantor set, the limit converges to a smaller value. Increasing the perturbation the gaps in the cantor set become larger and the value of the correlation dimension decreases even more.

We have calculated the correlation dimension of the last KAM curve iterating the initial value obtained with the Newton method 2048 times and dividing the curve in 500 intervals. This division determines the minimum value of l that the program can detect. In the figure (2.5) the values of the correlation dimension for the spectrum (2.67) with N=10 are shown for various values of ϵ.

	$\epsilon_{lyapunov}$	$\epsilon_{dim.corr.}$
standard map		
	0.690	0.682
linear decay		
N = 5	5.72 d-2	5.80 d-2
N = 10	1.9 d-2	1.85 d-2
exponential decay		
N = 5	2.70 d-2	2.60 d-2
N = 10	0.9 d-2	0.84 d-2

Table 1: critical perturbative parameter for various kinds of spectrum, calculated with the Lyapunov exponent and correlation dimension.

We have verified these methods, applying them to the standard map, normalized. It is a well known result [13] that the critical perturbation parameter is η=0.687.. (η=0.9716.., if non-normalized). In this case, the Lyapunov exponent has became positive at η=0.690 and the correlation dimension has began to decrease at η=0.682.

The results for the Generalized Standard Maps (2.67) and (2.66) are in the table 1, where in the column '$\epsilon_{lyapunov}$' we write the value of the perturbation parameter at which the lyapunov exponent became positive and in the column '$\epsilon_{dim.corr.}$', the value at which the correlation dimension begins to decrease.

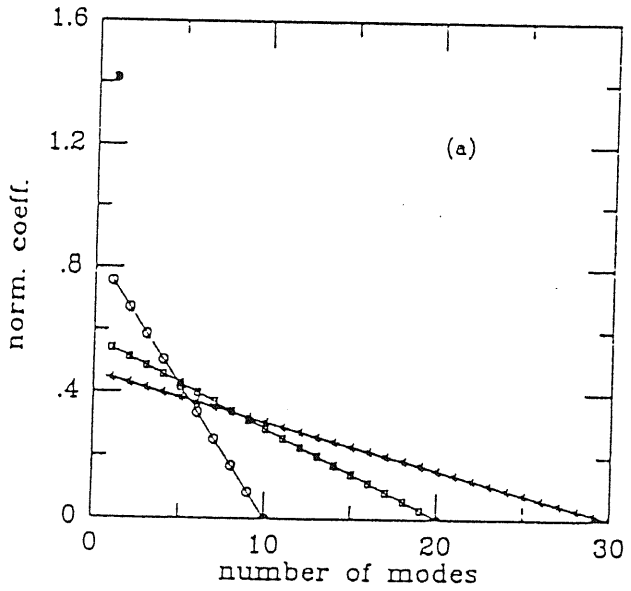

Figure 2.6: plot of the normalized spectrum (2.69) versus the number of modes, with N= 10, 20, 30

Using these two methods we were able to determine a range of the perturbative parameter, where the critical value can be. In order to have a more precise results, it is necessary to calculate the initial conditions to other values of perturbation, and calculate them with more accuracy. Also the correlation dimension should be calculated

with more points in the orbit and considering a smaller l. This means long CPU time. But the range we have obtained are narrow enough to let us say that the transition to stochasticity depends on the spectrum considered [27].

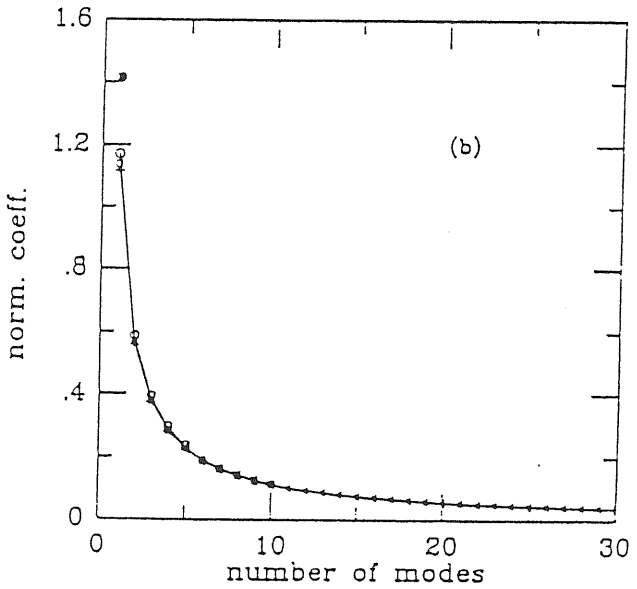

Figure 2.7: plot of the normalized spectrum (2.70) versus the number of modes, with N= 10, 20, 30.

In order to analyse the transition to stochasticity of spectra with a larger number of modes, we have used the Greene method. This method permits us to calculate an initial point of a convergent of the golden mean much more quicker than with the Newton method. In this method the break-up of a KAM curve with an irrational winding number w is associated with the destabilization of the orbits of the the elliptic fixed points with a rational winding number w' that approximates w. Details of this method are presented in the appendix C. Using the Greene method we analyzed [28] Generalized Standard Maps with the following perturbative spectra:

$$V(\psi_k) = \sum_{n=1}^{N} \frac{N-n}{N} \sin(\pi n \psi_k) \tag{2.69}$$

and

$$V(\psi_k) = \sum_{n=1}^{N} \frac{1}{n} \sin(\pi n \psi_k), \tag{2.70}$$

where N is always a finite number.

In the figures (2.6) and (2.7) these two spectra are plotted as a function of the number of modes N. The black point at $n = 1$ in both graphs represents the coefficient of the Standard Map. In the spectrum (2.69), the last coefficient is always null, so we must consider $N = 2$ to obtain the Standard Map.

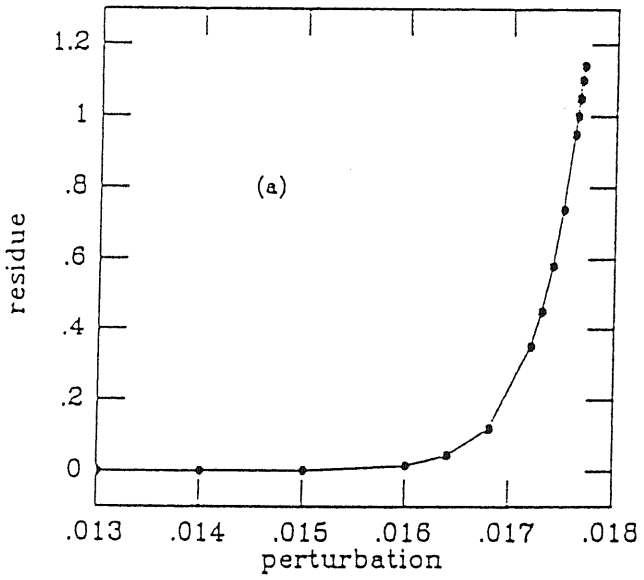

Figure 2.8: the residue for various values of perturbation. The case considered was the spectrum (2.69) with N=10.

We calculated the break-up of the curve associated with the golden mean in two independent ways: calculating its Lyapunov exponent and

residue. The residue is less than 1 when the periodic orbit is elliptic and greater than 1 when the periodic orbit is hyperbolic.

The results obtained using these two methods are consistent. In the figure (2.8) we can see the residue and in the figure (2.9) the Lyapunov exponent of the golden mean curve for the decay (2.69), with N=10, for various values of the perturbation. The value of the perturbation parameter, for which the residue becomes greater than 1 and the Lyapunov exponent positive, is the same.

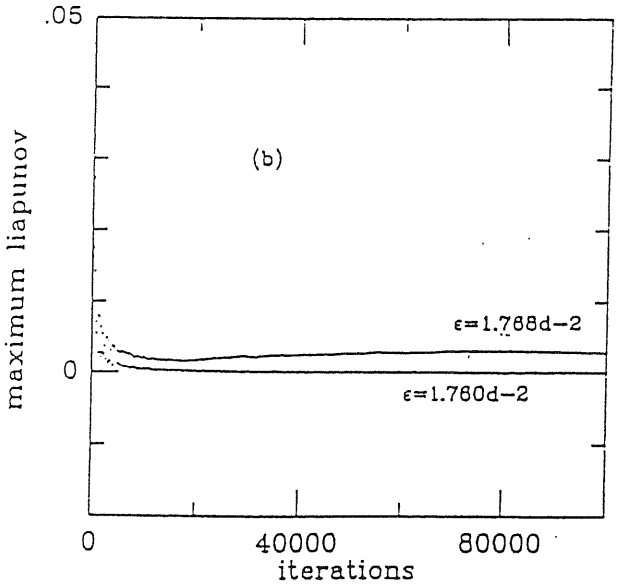

Figure 2.9: the Lyapunov exponent for various values of perturbation. The case considered was the spectrum (2.69) with N=10.

The critical parameter depends on the form of the coefficients of the spectrum and on the number of modes. The dependence on the number of modes seems to be the most relevant. In fact ϵ_c varies, on the both spectra, in a monotonic way by almost two orders of magnitude when we pass from $N = 5$ to $N = 30$.

A scaling law between the critical perturbation parameter and the number of modes is obtained in both spectra. In the figures (2.10) and

(2.11) we have plotted $-\log \epsilon_c$ as a function of N for the spectrum (2.69) and (2.70) respectively. It is clear that the critical value is a function of the number of modes, given by:

$$\epsilon_c(N) = \frac{N^{-A}}{C}, \tag{2.71}$$

where A and C are two constants that depend on the perturbative spectra.

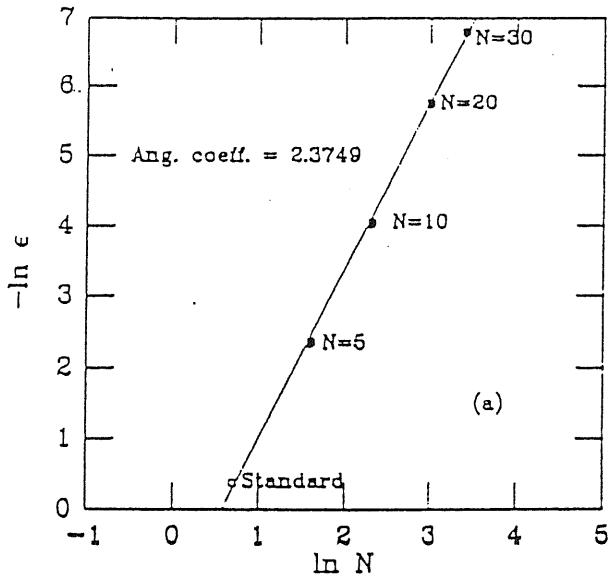

Figure 2.10: $-ln\epsilon \times lnN$ for the spectrum (2.69). Using the mean square method in both cases, we obtain a straight line and reproduce the known result of the Standard Map.

Using the mean square method we have calculated the values of A

$$A_a = 2.37 \qquad A_b = 1.61. \tag{2.72}$$

The values of C depend on the critical parameter of the Standard Map, ϵ_c^{ST}, and are

$$C_a = \frac{1}{\epsilon_c^{ST} 2^{A_a}} \qquad C_b = \frac{1}{\epsilon_c^{ST}}. \tag{2.73}$$

By comparing the critical value of the two spectra when both have the same number of modes we can observe that the difference of the coefficients affects the value of ϵ_c. But if we compare the value of ϵ_c of any one of the two spectra for different values of modes, we can see that the increase of the number of modes affects, more strongly, the critical value rather than the difference between the coefficients of the two spectra [28].

The dependence on the number of modes can be heuristically explained considering the Chirikov criterion of the threshold of stochasticity. When the number of modes of the perturbative spectrum increases, more resonances are possible, the width of the islands are larger and the overlap of them occurs at a smaller value of ϵ.

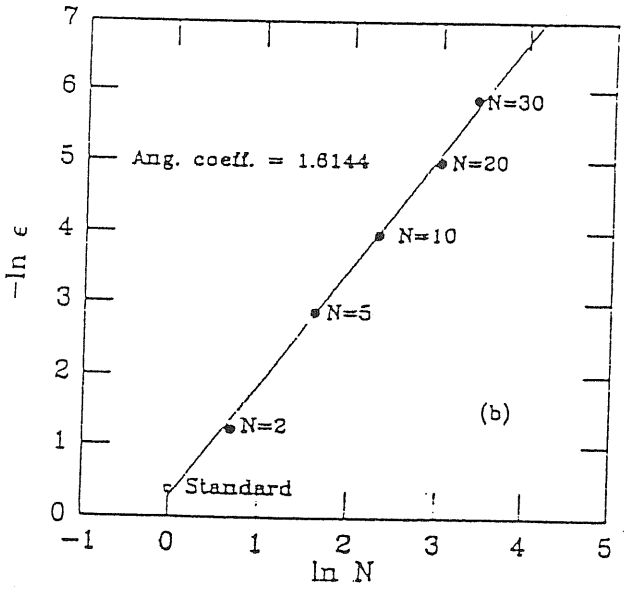

Figure 2.11: $-ln\epsilon \times lnN$ for the spectrum (2.70). Using the mean square method in both cases, we obtain a straight line and reproduce the known result of the Standard Map.

Chapter 3

Description of the Magnetic Field Lines by a Magnetohydrodynamic Code

3.1 Introduction

The "Reversed Field Pinch" (RFP) machine is a toroidal device of confinement of plasma by magnetic fields. In this device the axial magnetic field, B_z, and the poloidal magnetic field, B_θ, are of the same order of magnitude, and yield two useful parameters in the description of the RFP, that is, the pinch parameter, $\Theta = B_\theta|_{wall}/B_{zave}$ and the field reversal parameter, $F = B_z|_{wall}/B_{zave}$.

This machine derives its name from the fact that the plasmas exhibit robustly long lifetime when the axial magnetic field, B_z, at the outer border reverses direction relatively to the field on the axis (r=0) [32]. This state is achieved due to the application of an axial electric field that supplies the system with energy. It is a remarkable fact that after the reversal is achieved, all the RFP experiments are observed to seek approximately the same operating values of F, and Θ. Taylor [1] explained this behaviour in a global sense by assuming that the plasma naturally seeks its lowest energy state subject to the constraint that the axial magnetic flux and the magnetic helicity remain constant. This process is called relaxation. This simple variational calculation

yields force-free magnetic fields that exhibit axial field reversal whenever $\Theta > 1.2$. This is a simple and elegant theory that describes the global properties of the RFP. However, being of a variational nature, it does not adress the dynamical mechanisms responsible for the relaxation process and does not explain the anomalously long lifetime of RFP plasmas in the presence of finite plasma resistivity. The plasma can be maintained almost indefinitely at fixed values of F and Θ in the presence of an applied axial voltage, that supplies the system with poloidal flux. Poloidal flux is apparently dynamically converted into axial flux in sufficient amounts to maintain F and Θ at their proper values. This is called the RFP dynamo [32].

In order to understand the dynamics of the RFP dynamo and the behaviour of the magnetic profiles, numerical algorithms for the simulation of three-dimensional magnetohydrodynamic (MHD) systems have been done [32] - [37]. We developed one of these codes in cylindrical geometry. The mathematical model and numerical procedure used are presented in sections (3.2) and (3.3), respectively.

Our goal at this stage of development was to analyse the behaviour of the magnetic profiles at times of the order of the Alfvén times. We checked the code comparing the numerical and analytical time development of an Alfvén wave, then we evolve the system from a phenomenological magnetic profile without a supply of energy. We observed that the profiles decay and the initial reversal of the axial magnetic field was lost. This is the expected behaviour [6], since the axial magnetic flux is constant. These results are presented in section (3.4).

3.2 The Mathematical Model

The magnetohydrodynamic (MHD) equation we solved are given by:

$$\frac{\partial \mathbf{P}}{\partial t} = -\nabla.[\rho \mathbf{v}\mathbf{v} + (p + \frac{B^2}{2})\mathbf{I} - \mathbf{B}\mathbf{B} - \nu \nabla.\mathbf{v}] \tag{3.1}$$

$$\frac{\partial \mathbf{B}}{\partial t} = -\nabla \times \mathbf{E} \tag{3.2}$$

$$\mathbf{E} = -\mathbf{v} \times \mathbf{B} + \eta \mathbf{J} \tag{3.3}$$

$$\mathbf{J} = \nabla \times \mathbf{B} \tag{3.4}$$

where $\mathbf{P}$ is the momentum, $\mathbf{B}$ is the magnetic field in units of a characteristic value B_0, ρ is the density in units of a characteristic value ρ_0, p is the pressure in units of a characteristic value p_0. $\mathbf{v}$ is the velocity measured in units of the Alfvén velocity, $v_A = B_0/\sqrt{\rho_0}$. All the lengths are measured in units of a, that is the minor radius of the physical system. The time is measured in units of the Alfvén time, $t_A = a/v_A$. ν and η are the viscosity and resistivity and constant and uniform. In this code we considered the density uniform and constant. To evolve these equations in time we need to know their initial and boundary conditions. These are presented in the next sections.

3.2.1 Spectral Method and Finite Difference Aproximation

The equations (3.1), (3.2), (3.3) and (3.4) were solved [38], [39] in cylindrical coordinates (z, r, θ) in a mesh of $N_z \times N_r \times N_\theta$ grid points $(0 \leq z_i \leq 2\pi R, 0 \leq r_j \leq 1.0 \leq \theta_k \leq 2\pi)$. The spacing in the poloidal (θ) and axial (z) directions is uniform such that $\Delta\theta = \frac{2\pi}{N_\theta}$ and $\Delta z = \frac{2\pi R}{N_z}$, where R is the major axis of the toroid. The coordinate r has its values between 0 and 1 because it is normalized by a, that is the radius of the cylinder we are considering. The periodic nature of the equations (3.1), (3.2), (3.3) and (3.4) with respect to the coordinates allows a spectral representation to be employed.

Any generic function $u(z, r, \theta)$ periodic in the interval $(0 \leq z \leq 2\pi R, 0 \leq \theta \leq 2\pi)$ can be represented by the complex Fourier series [38], [39]:

$$u(z, r, \theta) = \sum_{m,n=-\infty}^{+\infty} u^{m,n}(r) e^{i(m\theta + nz)} \tag{3.5}$$

where the complex Fourier coefficients, $u^{m,n}(r)$, are given by:

$$u^{m,n}(r) = \int_0^{2\pi} \frac{d\theta}{2\pi} \int_0^{2\pi R} \frac{dz}{2\pi R} u(z, r, \theta) e^{-i(m\theta + nz)}. \tag{3.6}$$

The reality of $u(z, r, \theta)$ requires that

$$u^{m,n} = (u^{-m,-n})^*. \tag{3.7}$$

When the function is described by $N_z \times N_\theta \times N_r$ grid points, as in our case, it can be represented by the finite Fourier series:

$$u(z_i, r_j, \theta_k) = \sum_{n=-\frac{N_z}{2}+1}^{\frac{N_z}{2}} \sum_{m=-\frac{N_\theta}{2}+1}^{\frac{N_\theta}{2}} u^{m,n}(r_j) e^{i(m\theta_k + nz_i)} \tag{3.8}$$

with

$$u^{m,n}(r_j) = \frac{1}{N_z N_\theta} \sum_{i=1}^{N_z+1} \sum_{k=1}^{N_\theta+1} u(z_i, r_j, \theta_k) e^{-i(m\theta_k + nz_i)} \tag{3.9}$$

where $z_i = (i-1)\frac{2\pi R}{N_z}$ and $\theta_k = (k-1)\frac{2\pi}{N_\theta}$.

The radial coordinate is treated by the method of finite differences. The spacing in this coordinate is uniform and given by $\Delta r = \frac{1}{N_r}$.

3.2.2 Boundary Conditions

The walls were considered perfectly conducting [40]. This means that the tangencial components of the eletric field at $r = 1$ and the radial component of the magnetic field are null [41], that is:

$$E_z(r=1) = E_\theta(r=1) = 0 \tag{3.10}$$

$$B_r(r=1) = 0 \tag{3.11}$$

for all modes. For the velocity we considered that $\mathbf{v}(r=1) = 0$ for all modes. The condition $v_r(r=1) = 0$ is obtained from Ohm's equation.

The system we are considering has viscosity and resistivity that damp it. If we evolve the system in time just with the boundary conditions given above, we will observe that the magnitude of the components of the magnetic field and velocity diminish with the time [6]. Consequently, the components of the current also diminish. In the experiments, the system is supplied with energy that maintains it, despite

the damping. One way of doing this in our code is to apply appropriate boundary conditions such that the total mean axial current, I_z, is keeped constant.

The total mean axial current is given by:

$$< I_z >= 2\pi \int_0^1 r < J_r > dr, \tag{3.12}$$

where J_z is the axial component of the density current, and $< J_z >$ means the averaged value with respect with z and θ, that is, the component $n = 0$ and $m = 0$ of J_z. $< J_z >$ is given by

$$< J_z >= \frac{1}{r}[\frac{\partial}{\partial r}(rB_\theta^{0,0}) - \frac{\partial B_r^{0,0}}{\partial \theta}]. \tag{3.13}$$

Substituing equation (3.13) in (3.12) we obtain for the total mean axial current:

$$< I_z >= 2\pi B_\theta^{0,0}(r = 1). \tag{3.14}$$

The equation (3.14) shows us that if we keep constant $B_\theta^{0,0}$ at $r = 1$, the total mean axial current will also be keeped constant. This is the boundary condition we use, when we want to supply the system with energy.

3.2.3 Initial Configuration

One possibility of initial configuration could be the magnetic profiles given by the Taylor theory of relaxed state [1], that was presented in section (2.2.1) of this thesis. According to this theory, the equilibrium state of a slightly resistive turbulent plasma is given by the state that minimizes the magnetic energy and keeps the total helicity constant. For a plasma in a perfectly conducting wall, this equilibrium state is given by the force-free equation

$$\nabla \times \mathbf{B} = \mu \mathbf{B} \tag{3.15}$$

where μ is a constant.

The physical system we are considering is a plasma contained in a toroidal machine. Considering that the major radius is much greater

than the minor one, we can approximate this toroid by a cylinder and in this case the solution of equation (3.15) is given by the Bessel Fuction Model:

$$B_r = 0 \tag{3.16}$$

$$B_z = B_0 J_0(\mu r/a) \tag{3.17}$$

$$B_\theta = B_0 J_1(\mu r/a) \tag{3.18}$$

Knowing these components of the magnetic field, and expanding the Bessel function, we can write the security factor, $q(r)$, as a polynomial in r:

$$q_{Bessel}(r) = \frac{rB_z(r)}{RB_\theta(r)} = q_0(1 + a_1 r^2 + a_2 r^4) \tag{3.19}$$

The profiles of the Bessel Function Model describe very well the ones observed in the experiences, except in the region of r very close to 1. Due to this fact we did not use these profiles for the initial configuration of the magnetic fields, but magnetic profiles $B_z(r)$ and $B_\theta(r)$ that are numerically obtained from a phenomenological security factor $q(r)$ that differs from $q_{Bessel}(r)$ in the region of r close to 1. In this case the parameters q_0, a_1 and a_2 are not obtained from the expansion of the Bessel functions, but are phenomenological ones.

Another difference with the Bessel Function Model is that μ is not a constant, but a function of the radius $\mu(r)$.

From the phenomenological security factor $q(r)$ and the equation (3.15), we obtain:

$$\mu(r) = \frac{\frac{R}{a}[2q_0(1 - a_2 r^4)]}{r^2 + (\frac{R}{a})^2 q^2(r)} \tag{3.20}$$

Substituing $q(r)$ and $\mu(r)$ in equation (3.15), we obtain a differential equation to $B_z(r)$:

$$\frac{\partial B_z(r)}{\partial r} = -(\frac{a}{R})\frac{r\mu(r)}{q(r)} B_z(r), \tag{3.21}$$

that is solved numerically. The component $B_\theta(r)$ is obtained from the equation of the phenomenological security factor. As the initial magnetic profile is considered as an equilibrium one, the profiles obtained numerically are averaged with respect to z and θ and have just the component $m = n = 0$ different from zero. All other modes are null. The component $B_r(r)$ is null for all values of m and n.

For the same reasons, all the components of the velocity should be null. But it is convenient to use an initial velocity profile small in comparison with the initial magnetic profile, with valus of m and n different from zero, because this permits us to avoid initial transients and observe quicker the magnetic modes that grow.

The components of the initial profile of the velocities were given in the Fourier space of the coordinate z, for all values of n, with a random phase and an amplitude that diminuishes with the increasing of n:

$$V_z^n(r_j, \theta_k) = r_j^2(1 - r_j^2)cos(2\theta_k)\frac{1}{(1-n^2)^2}\exp^{iRD} \tag{3.22}$$

$$V_r^n(r_j, \theta_k) = r_j^2(1 - r_j^2)cos(\theta_k)\frac{1}{(1-n^2)^2}\exp^{iRD} \tag{3.23}$$

$$V_\theta^n(r_j, \theta_k) = r_j^2(1 - r_j^2)cos(\theta_k)\frac{1}{(1-n^2)^2}\exp^{iRD} \tag{3.24}$$

where RD is a random number.

After transforming to the configuration space, they were divided by their mean value with respect with θ and z, calculated at the value of the radius where the function $r^2(1-r^2)$ is a maximum. These functions are zero for $r = 0$ and $r = 1$. The velocities are given by:

$$V_l(z_i, r_j, \theta_k) = \epsilon\frac{V_l(z_i, r_j, \theta_k)}{< V_l(z_i, r_j^{max}, \theta_k) >} \tag{3.25}$$

where,

$$< V_l(z_i, r_j^{max}, \theta_k) >= \sqrt{\frac{\sum_{z_i,\theta_k}[V_l(z_i, r_j^{max}, \theta_k)]^2}{N_z N_\theta}} \tag{3.26}$$

ϵ is an input parameter of the order of 10^{-2}, l is representing the components z, r, θ, and $r_j^{max} = 0.5\sqrt{2}$.

3.3 Numerical Procedure

The calculation of the equations (3.1), (3.2), (3.3) and (3.4) using the spectral method and finite difference approximation requires some technical procedures to calculate the derivatives, to regularize the functions at $r = 0$ and to advance them in time.

As the equations are solved in cylindrical coordinates, the periodicity in the coordinates z and θ allows the spectral method to be applied and the derivatives with respect with these coordinates are easily computed in Fourier space. Due to the fact that the equations are not periodic in r, some approximations must be done to calculate the derivative with respect to r. The methods used to calculate all the derivatives are discussed in section 1.3.1.

The geometry of the system implies some regularity conditions to be imposed on the functions. As we are dealing with a cylindrical system, the functions must be invariant with respect to rotations in θ, at $r = 0$. This is one kind of regularization. Another one is when we must calculate the ratio $u(r)/r$ at $r = 0$. The fluxes are calculated in the Fourier space of the coordinates z and θ and these regularizations are done imposing some conditions on the Fourier coefficients. This is discussed in the section 1.3.2.

In our code we implemented two methods of time advancement: Adams-Bashfort and Runge-Kutta of third order. They are discussed in section 1.3.3.

3.3.1 Derivatives

Given a generic function $u(z_i, r_j, \theta_k)$, the derivatives $\frac{\partial u}{\partial \theta}$ and $\frac{\partial u}{\partial z}$ at the point (z_i, r_j, θ_k) are given by [39]:

$$\frac{\partial u}{\partial z}|_{(z_i,r_j,\theta_k)} = \sum_{m=\frac{-N_\theta}{2}+1}^{\frac{N_\theta}{2}} \sum_{n=\frac{-N_z}{2}+1}^{\frac{N_z}{2}} inu^{m,n}(r)e^{i(m\theta_k+nz)} \tag{3.27}$$

$$\frac{\partial u}{\partial \theta}|_{(z_i,r_j,\theta_k)} = \sum_{m=\frac{-N_\theta}{2}+1}^{\frac{N_\theta}{2}} \sum_{n=\frac{-N_z}{2}+1}^{\frac{N_z}{2}} imu^{m,n}(r)e^{i(m\theta_k+nz)}. \tag{3.28}$$

The derivative in the r coordinate is calculated in the finite difference approximation [42] and is expressed as a linear combination of the given function values. The finite difference approximation to the first derivative $\frac{du(r_j)}{dr}$ at the node j depends on the function values at the nodes near j. For second and fourth order central differences, the approximation for the derivative u'_j depends on the sets (u_{j-1}, u_{j+1}) and $(u_{j-2}, u_{j-1}, u_{j+1}, u_{j+2})$ respectively. Here we used the notation that $u(r_j) \equiv u_j$. We used a scheme for the derivative that is a generalization of the Padé scheme, and is a one-parameter family of fourth-order accurate schemes given by:

$$u'_{j-1} + \alpha u'_j + u'_{j+1} = \frac{1+2\alpha}{3\Delta r}(u_{j+1} - u_{j-1}) + \frac{4-\alpha}{12\Delta r}(u_{j+2} - u_{j-2}) \quad (3.29)$$

We used $\alpha = 4$ that is the classical fourth-order Padé formula. This is a tridiagonal scheme, and the truncation error is given by

$$\frac{4}{5!}(3\alpha - 1)(\Delta r)^4 u^{(5)}. \quad (3.30)$$

The derivatives at the boundary nodes $j = 1(r = 0)$ and $j = N_r(r = 1)$ must be calculated using appropriate additional relations because the system does not present periodicity in r.

At $r = 0$ we can use the fact that all the functions involved in this code have a well-defined parity. The fluxes are calculated in the Fourier space, so we are always doing differentiations of the Fourier coefficients and we need to know the parity of these coefficients.

Any function represented by a finite Fourier series:

$$u(z_i, r_j, \theta_k) = \sum_{m=-\frac{N_\theta}{2}+1}^{\frac{N_\theta}{2}} \sum_{n=-\frac{N_z}{2}+1}^{\frac{N_z}{2}} u^{m,n}(r) e^{i(m\theta_k + nz)}. \quad (3.31)$$

can have its coefficients written as a serie in r:

$$u^{m,n}(r_j) = \sum_{l=0}^{N} a_l^{m,n} r_j^l \quad (3.32)$$

If the function $u(z_i, r_j, \theta_k)$ is even, the function $r^l e^{im\theta_k}$ is a polynomial if and only if [43]

$$l - m \in 2\mathbf{Z} \tag{3.33}$$

and

$$l \geq |m|. \tag{3.34}$$

Applying these conditions on (3.32), the Fourier coefficient can be rewritten as

$$u^{m,n}(r_j) = \sum_{l=0}^{N} a_l^{m,n} r^{2l+m}. \tag{3.35}$$

We see that if m is even or odd, the coefficient is even or odd respectively.

On the other hand, if $u(z_i, r_j, \theta_k)$ is odd, the conditions on the exponents l and m are different. In this case $r^l e^{im\theta_k}$ is a polynomial if and only if [43]

$$l - m \in 2\mathbf{Z} + 1 \tag{3.36}$$

and $l \geq |m|$.

Applying these conditions on (3.32), we can rewrite the Fourier coefficient as

$$u^{m,n}(r_j) = \sum_{l=0}^{N} a_l^{m,n} r^{2l+m+1}. \tag{3.37}$$

From equation (3.37) it is possible to see that if m is even or odd, the coefficient is odd or even respectively.

When we are calculating the r derivative of an odd Fourier coefficient, we can use the fact that for an odd function

$$\frac{du(r)}{dr} = \frac{du(-r)}{dr} \tag{3.38}$$

$$u(r) = -u(-r) \tag{3.39}$$

and write

$$2u_1' + u_2' = \frac{3}{\Delta r}u_2 \tag{3.40}$$

For an even Fourier coefficient, we know that $u'(r=0) = 0$.
At the other border, $r = N_r$, we used a third-order scheme

$$4u'_{N_r-1} + 2u'_{N_r} = 5u_{N_r} - 4u_{N_r-1} - u_{N_r-2}. \tag{3.41}$$

3.3.2 Regularization at $r = 0$

We used two kinds of regularization at $r = 0$ in this code. One of them is the conditions we must impose on the Fourier coefficients of the function in order that the function be invariant with respect with θ at $r = 0$, that is [39]

$$\frac{\partial \mathbf{u}}{\partial \theta}|_{r=0} = 0. \tag{3.42}$$

The functions involved in this code are vectorial and have the components $\mathbf{e}_z, \mathbf{e}_r, \mathbf{e}_\theta$:

$$\mathbf{u}(z,r,\theta) = u_z(z,r,\theta)\mathbf{e}_z + u_r(z,r,\theta)\mathbf{e}_r + u_\theta(z,r,\theta)\mathbf{e}_\theta \tag{3.43}$$

The component $u_z(z,r,\theta)$ acts as a scalar because $\mathbf{e}_z$ does not depend on θ. Given this function

$$u_z(z_i,r_j,\theta_k) = \sum_m u_z^m(z_i,r_j)e^{im\theta_k}, \tag{3.44}$$

applying the condition (3.42) we have:

$$\frac{\partial u_z}{\partial \theta_k}(z_i,r_j,\theta_k) = \sum_m imu_z^m(z_i,r_j)e^{im\theta_k}|_{r=0} = 0. \tag{3.45}$$

In order the equation (3.45) be satisfied, the following condition must be imposed:

$$u_z^m(z_i,r_j)|_{r=0} = 0 \tag{3.46}$$

for $m \neq 0$. For $m = 0$ we have the condition:

$$\frac{du_z^m}{dr}(z_i, r_j)|_{r=0} = 0, \tag{3.47}$$

that is coeherent with the fact that the scalar function is an even function.

When the condition $\frac{d\mathbf{u}}{d\theta}$ is applied on the components r and θ, they act as a vector because $\mathbf{e}_r$ and $\mathbf{e}_\theta$ depend on θ. The results we obtain are

$$u_r^m|_{r=0} = u_\theta^m|_{r=0} = 0 \tag{3.48}$$

for $|m| \neq 1$, and

$$(u_r^m + i|m|u_\theta^m)|_{r=0} = 0 \tag{3.49}$$

for $|m| = 1$.

Another regularity condition at $r = 0$ is imposed when there is an expression of the kind $\frac{f(r)}{r}$. All the fluxes are calculated in the Fourier space and also these regularity conditions are imposed on the Fourier coefficients.

The Fourier coefficients of an even function are given by [43]:

$$u^m(r) = r^m \sum_{l=0, l_{even}}^{N} a_l r^l. \tag{3.50}$$

The even functions in this code are the B_z, v_z, ρ and p. ρ and p are considered uniform and constant. In our case, the component $m = 0$ of v_z is zero at $r = 0$, so the summation of l begins in $l = 2$ for $m = 0$. For other values of m the summation begins at $l = 0$. On the other hand, the component $m = 0$ of B_z is not zero at $r = 0$. But we do not have in any of the equations an expression of the kind $\frac{B_z}{r}|_{r=0}$. We have $\frac{1}{r}\frac{\partial B_z}{\partial \theta}|_{r=0}$ that is zero for $m = 0$. So, when we have an expression $\frac{u(r)}{r}$, where $u(r)$ is even, we have that:

$$\frac{u^m(r)}{r}|_{r=0} = 0 \tag{3.51}$$

for $|m| \neq 1$, and

$$\frac{u^m(r)}{r} = \frac{\partial u^m(r)}{\partial r}|_{r=0} \tag{3.52}$$

for $|m| = 1$.

The Fourier coefficient of an odd function is given by

$$u^m(r) = r^{m+1} \sum_{l=0,l_{even}}^{N} a_l r^l \tag{3.53}$$

and when we have an expression of the kind $\frac{u(r)}{r}$ where $u(r)$ is odd, we have that

$$\frac{u^m(r)}{r}|_{r=0} = 0 \tag{3.54}$$

for $m \neq 0$, and

$$\frac{u^m(r)}{r} = \frac{\partial u^m(r)}{\partial r}|_{r=0} \tag{3.55}$$

for $m = 0$.

3.3.3 Time Integration

In this code it is possible to choose between two methods of time advancement [44]. One of them is the second-order method, called Adams-Bashforth and that is given by

$$u^{k+1}(z,r,\theta) = u^k(z,r,\theta) - \frac{\Delta t}{2}[3F^k(z,r,\theta) - F^{k-1}(z,r,\theta)] \tag{3.56}$$

where the flux is $\frac{\partial u}{\partial t} = -F(u)$ and $u^k(z,r,\theta)$ is the function $u(z,r,\theta)$ calculated at the time step k.

Another method is one member of a family of explicity third-order Runge-Kutta schemes. Given a flux $\frac{\partial u}{\partial t} = -F(u)$, the advancement in time is given by

$$u^{k+1}(z,r,\theta) = u^k(z,r,\theta) - \Delta t[c_{k'}F^k(z,r,\theta) + d_{k'}F^{k-1}(z,r,\theta)] \tag{3.57}$$

where k is the substep number, $k' = 1 + mod(k, K)$ is the substep number within a time step Δt and K is the number of substeps in a time step.

In our case we used

$$K = 3, \tag{3.58}$$

$$c_1 = 8/15, d_1 = 0, \tag{3.59}$$

$$c_2 = 5/12, d_2 = -17/60, \tag{3.60}$$

$$c_3 = 3/4, d_3 = -5/12. \tag{3.61}$$

One advantage of the Runge-Kuttta scheme in comparison with Adams-Bahsforth is that it is self-starting ($d_1 = 0$), while the other requires a separate method for the first time step. This property allows one to change Δt at the begining of every time step.

The time step was calculated using a stability algorithm [38] which compared the time steps associated with the viscosity velocity on one hand and Alfven and sound velocity on the other. Associated with the viscosity velocity we have:

$$T_1 = \frac{3}{8} KK min_j [\frac{\rho(rd\theta)^2}{\nu(r_j)}, \frac{\rho(dr)^2}{\nu(r_j)}] \tag{3.62}$$

if there is viscosity ($\nu(r) \neq 0$). If $\nu = 0$, this time step is given by

$$T_1 = KK. \tag{3.63}$$

The time step associated with the Alfven and sound velocities is

$$T_2 = \frac{KK}{max[\frac{a_z}{dz} + \frac{a_r}{dr} + \frac{a_\theta}{d\theta}]} \tag{3.64}$$

where

$$a_i = |v_i| + \sqrt{c_s^2 + v_a^2}, \tag{3.65}$$

$i = z, r, \theta$, c_s is the local sound velocity

$$c_s = \frac{\gamma(\gamma-1)E}{\rho} \tag{3.66}$$

where γ is the ratio of specific heats and v_a is the Alfven velocity,

$$v_a^2 = \frac{B_z^2 + B_r^2 + B_\theta^2}{\rho}. \tag{3.67}$$

The time step used was the smallest of T_1 and T_2:

$$T = min(T_1, T_2). \tag{3.68}$$

The constant KK is associated with the time integration scheme that we are using.

3.4 Results

3.4.1 Alfvén wave

We used as a test of this code a comparison between the numerical time evolution of a Alfvén wave and the analytic one. The analytic behaviour was obtained linearizing the ideal MHD equations:

$$\frac{\partial \mathbf{B}}{\partial t} = \nabla \times [\mathbf{v} \times \mathbf{B}] \tag{3.69}$$

$$\rho \frac{\partial \mathbf{v}}{\partial t} = -\nabla.[\rho \mathbf{v}\mathbf{v} + (p + \frac{B^2}{2})\mathbf{I} - \mathbf{B}\mathbf{B}] \tag{3.70}$$

We linearize these equations substituing in them the expressions:

$$\mathbf{v} = \mathbf{v}^{(0)} + \epsilon \mathbf{v}^{(1)} + O(\epsilon^2) \tag{3.71}$$

$$\mathbf{B} = \mathbf{B}^{(0)} + \epsilon \mathbf{B}^{(1)} + O(\epsilon^2) \tag{3.72}$$

where ϵ is a perturbative parameter. We keep terms of $O(\epsilon)$.

Considering that we used as initial configuration

$$v_\theta^{(1)} = r(1-r^2)cos(z) \tag{3.73}$$

$$B_z^{(0)} = 1.0, \tag{3.74}$$

all other terms are null. We obtain for the linearized equations:

$$\frac{\partial B_r^{(1)}}{\partial t} = 0 \tag{3.75}$$

$$\frac{\partial B_\theta^{(1)}}{\partial t} = B_z^{(0)} \frac{\partial v_\theta^{(1)}}{\partial z} \tag{3.76}$$

$$\frac{\partial B_z^{(1)}}{\partial t} = 0 \tag{3.77}$$

$$\rho \frac{\partial v_z^{(1)}}{\partial t} = \frac{B_z^{(0)}}{r} \frac{\partial B_\theta^{(1)}}{\partial \theta} \tag{3.78}$$

$$\rho \frac{\partial v_r^{(1)}}{\partial t} = 0 \tag{3.79}$$

$$\rho \frac{\partial v_\theta^{(1)}}{\partial t} = B_z^{(0)} \frac{\partial B_\theta^{(1)}}{\partial \theta} \tag{3.80}$$

The time evolution of the component $v_\theta^{(1)}$ is given by the equation:

$$\rho \frac{\partial^2 v_\theta^{(1)}}{\partial t^2} = B_z^{2(0)} \frac{\partial^2}{\partial z^2} v_\theta^{(1)}. \tag{3.81}$$

which solution is

$$v_\theta^{(1)} = \sum_{m,n} v_\theta^{m,n(1)}(r) e^{i(m\theta + nz)} e^{iwt \frac{B_0}{\sqrt{\rho}}}, \tag{3.82}$$

We can see that the frequency is given by $w = n$.

We can observe in the figure (3.1) the value of lnI versus the time (normalized by the Alfvén time), where I is given by:

$$I = \int |V_\theta^{0,1}|^2 dr \tag{3.83}$$

As the frequency is given by $w = n$ and in this case $n = 1$, the periody is $T = 2\pi$. In the figure we can see that the periody obtained with the numerical calculation is $T = 6.25$, in close agreement with the analytical results.

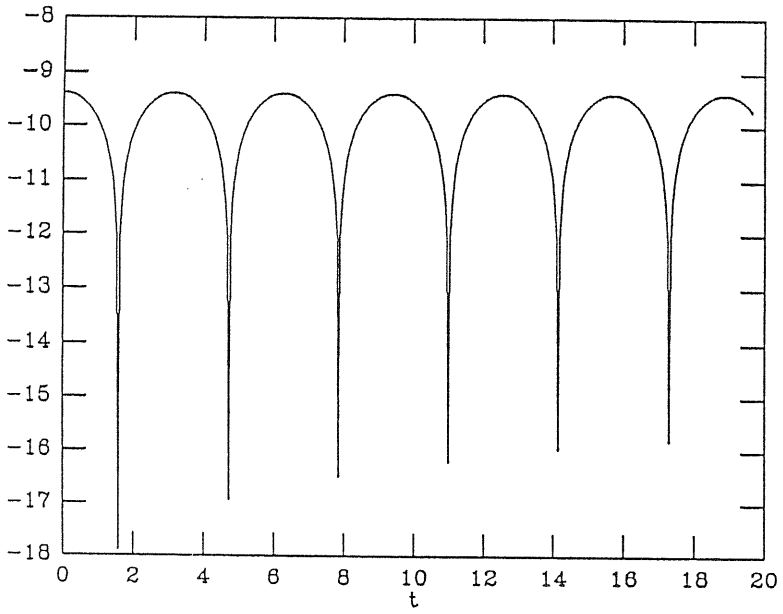

Figure 3.1: value of $ln(\int |v_\theta^{0,1}|^2 dr)$ versus the time. The periody of this Alfvén wave is T=6.25, in good agreement with the analytical results.

3.4.2 Time Evolution of the Magnetic Profiles

We evolved the MHD equations in time imposing just the boundary condition that the wall was perfectly conducting. We considered as initial conditions for the magnetic profiles the ones obtained numerically from the following security factor:

$$q(r) = 0.1255(1 - 1.8748r^2 + 0.8323r^4). \tag{3.84}$$

The aspect ratio, R/a, was equal to 5 and we used 48 radial, 32 poloidal and 8 axial mesh points. The normalized viscosity and resistivity were uniform, constant and equal to 0.2 and 0.1 respectively. The value of the parameter ϵ that multiplies the initial profiles of the velocities was 0.01. The time integration was performed with the Runge-Kutta method and the parameter $KK = 1$.

In the figures (3.2) - (3.7) we can see the time evolution of the modes $B_z^{0,0}$, $B_r^{1,0}$, $B_\theta^{0,0}$, $v_z^{1,0}$, $v_r^{1,0}$ and $v_\theta^{1,0}$. The modes $m = n = 0$ of B_r and v are null in this case.

The system is not supplied with energy and the magnetic profiles decay due to resistivity. The walls are considered perfectly conducting and this implies that the axial magnetic flux is constant. The axial magnetic component losses its reversal in time because it decays keeping the flux constant. This is measured by the F parameter, that is negative at the begining and then becomes positive, always growing. In the present case the Θ parameter is a decreasing function, reflecting the decay of $B_\theta^{0,0}$. The time evolution of the axial magnetic flux, F and Θ parameters can be seen in figures (3.8), (3.9) and (3.10) respectively.

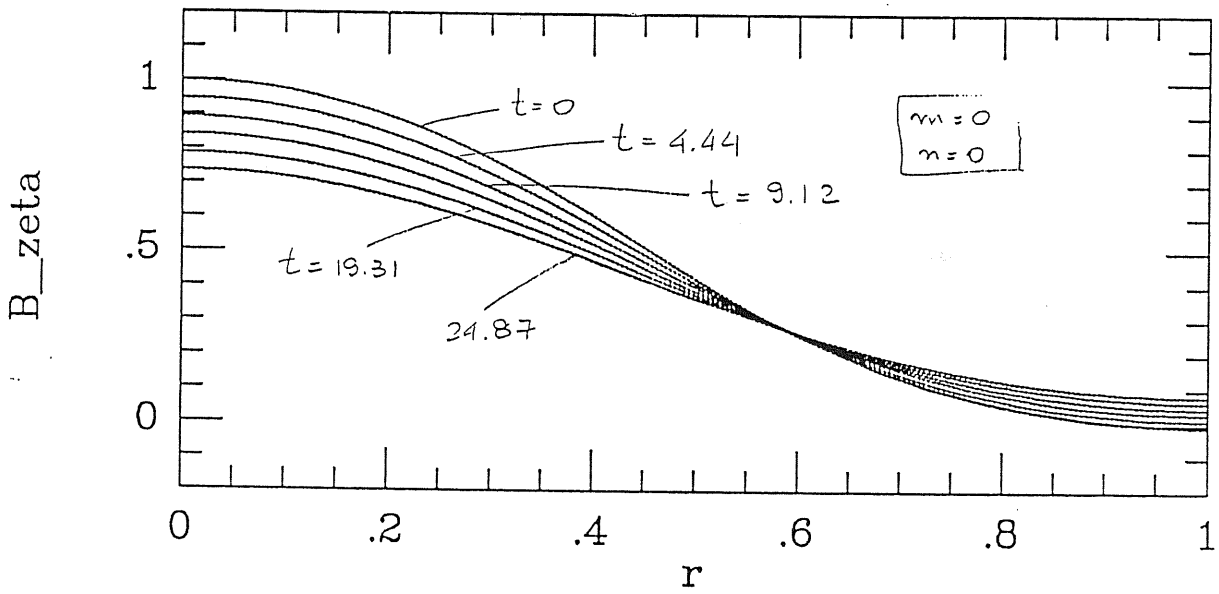

Figure 3.2: time evolution of the component $B_z^{0,0}$

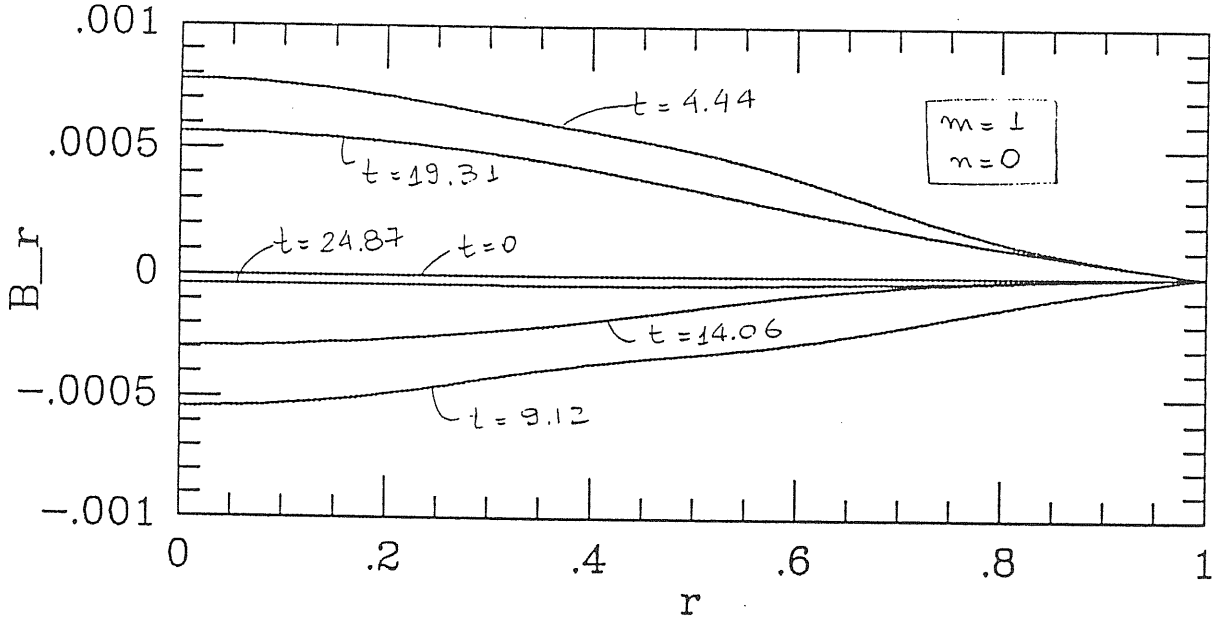

Figure 3.3: time evolution of the component $B_r^{1,0}$

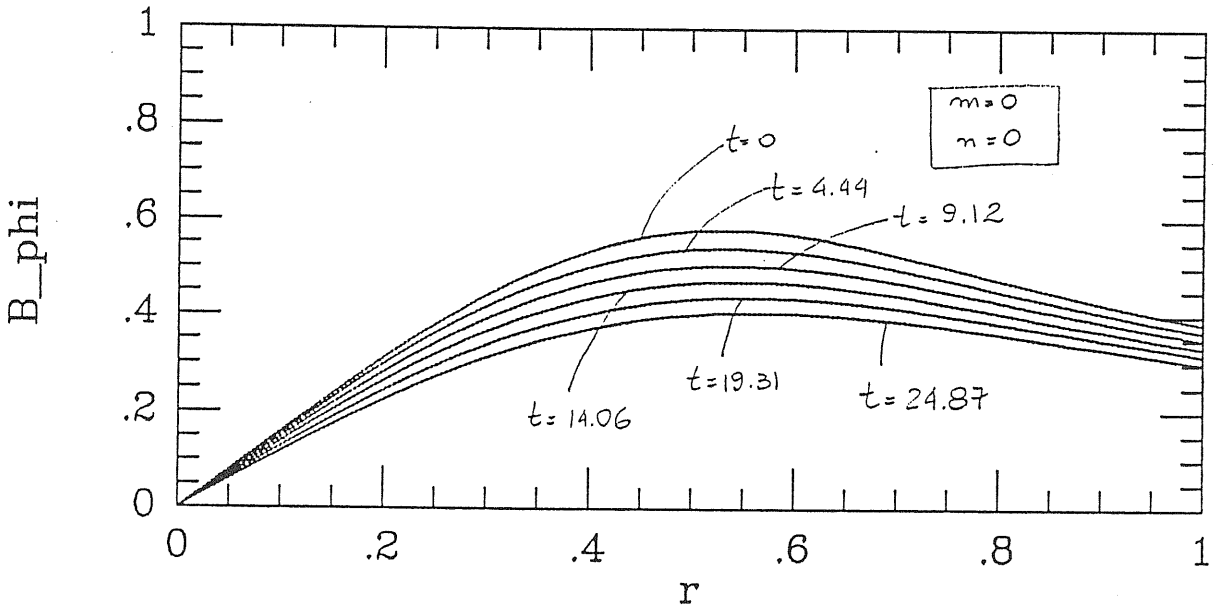

Figure 3.4: time evolution of the component $B_\theta^{0,0}$

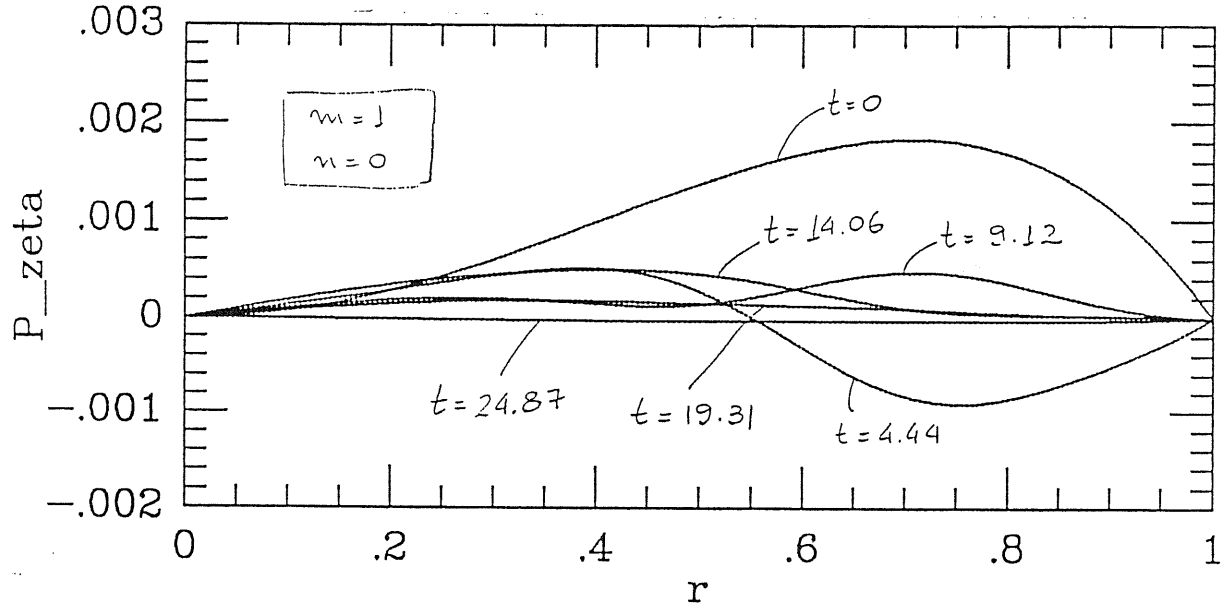

Figure 3.5: time evolution of the component $v_z^{1,0}$

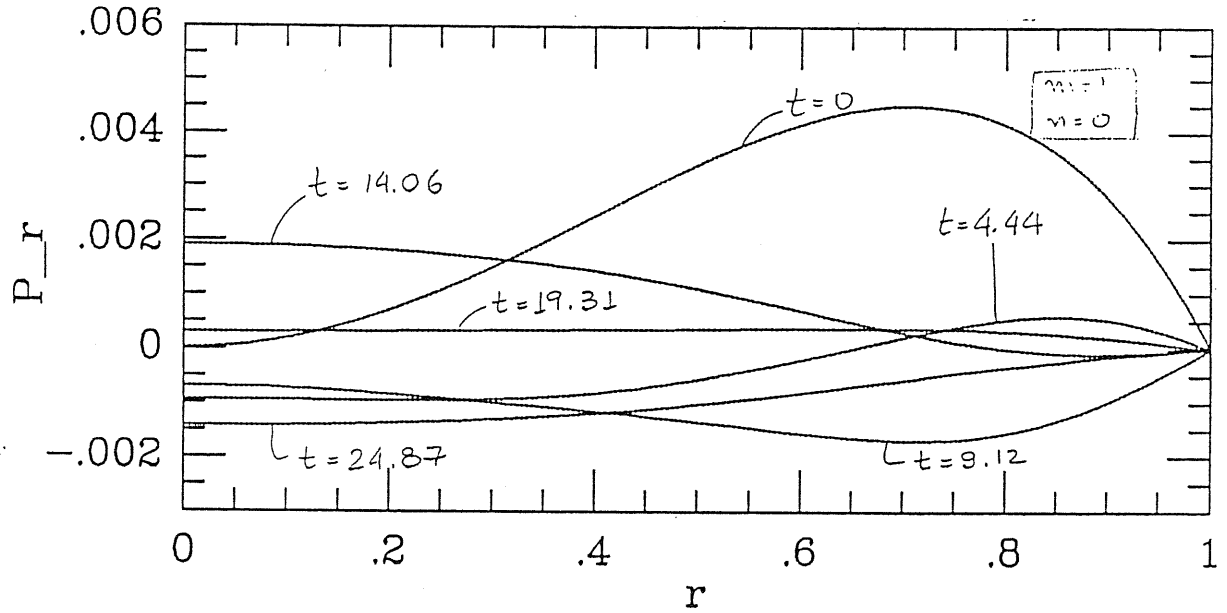

Figure 3.6: time evolution of the component $v_r^{1,0}$

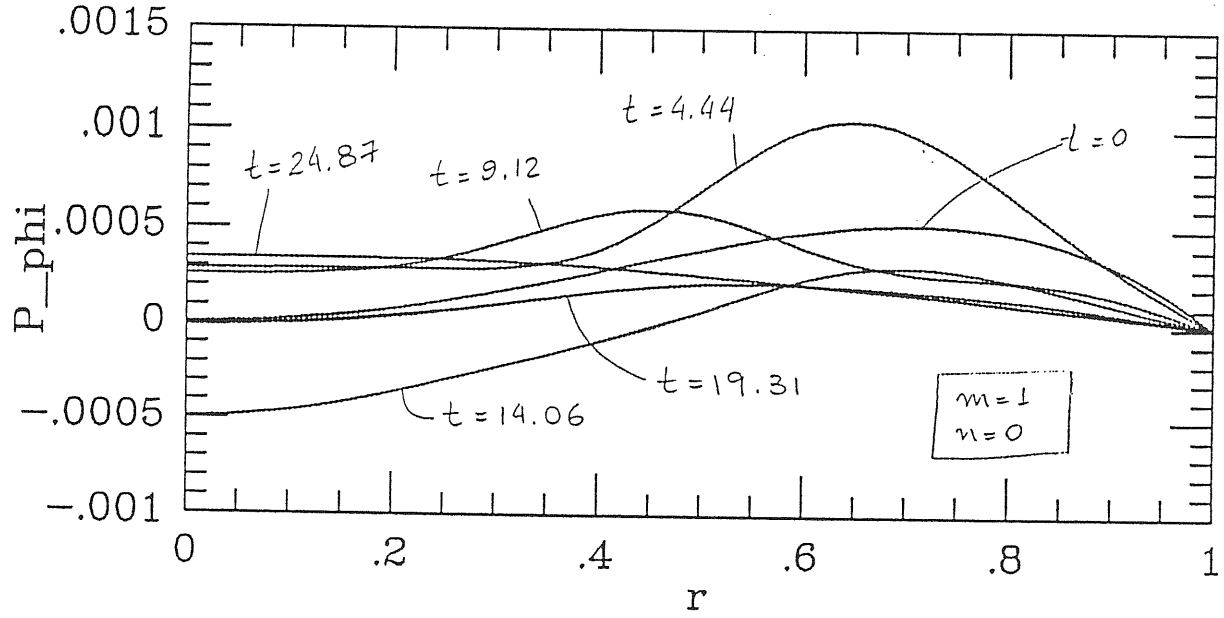

Figure 3.7: time evolution of the component $v_\theta^{1,0}$

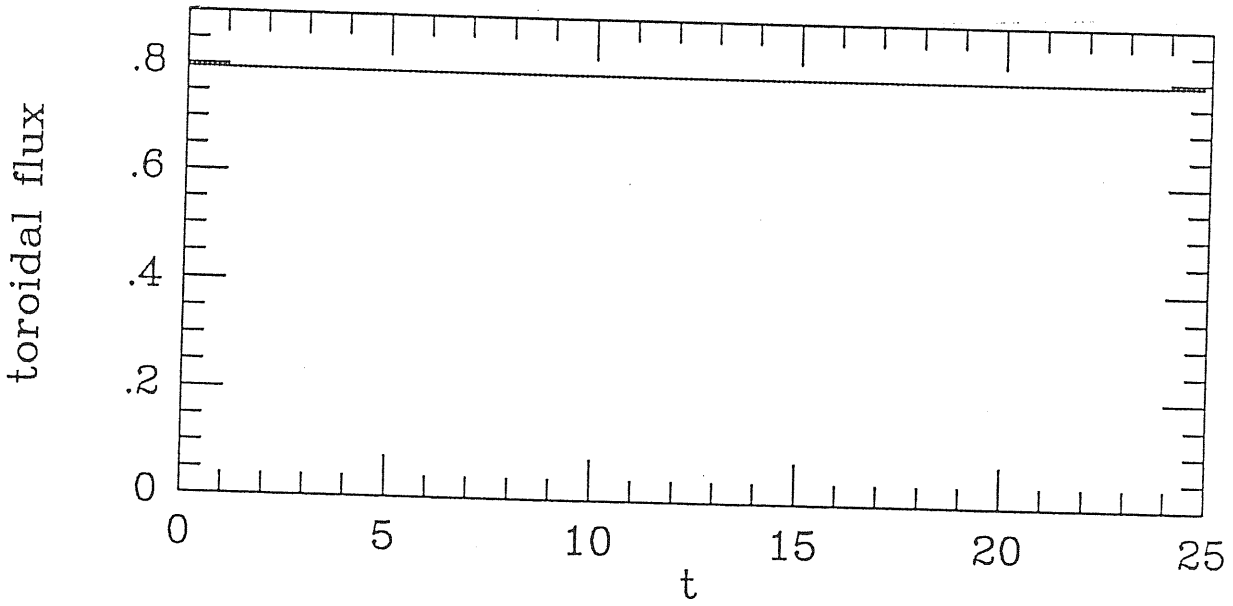

Figure 3.8: time evolution of the axial magnetic flux

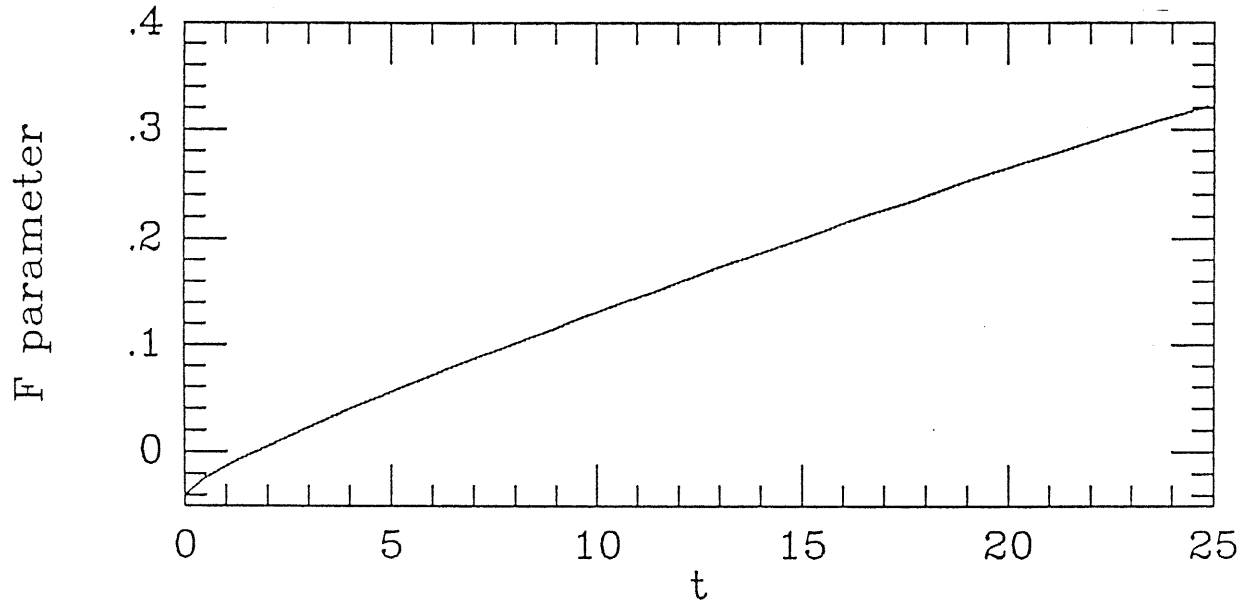

Figure 3.9: time evolution of the F parameter

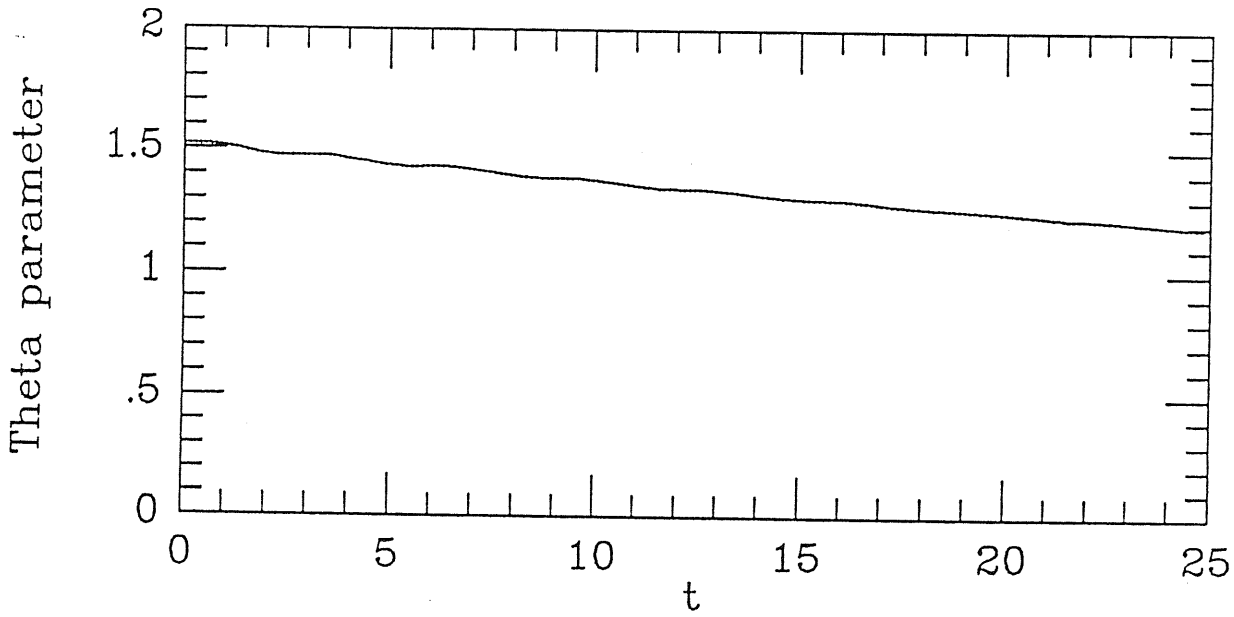

Figure 3.10: time evolution of the Θ parameter

Chapter 4

Self-Consistent Approach

4.1 Introduction

The magnetic field lines of a "Reversed Field Pinch" configuration can be described by a set of Generalized Standard Maps, as it was shown in the chapter 2. Due to this fact, it was possible to study the effect of different perturbative spectra of the magnetic field on the stability and diffusion of the magnetic profiles.

The time evolution of the magnetic profiles is given by the three-dimemsional MHD code, that was presented in the chapter 3. In order to take into account the effect of the perturbative spectra of the magnetic field on the time evolution of the magnetic profile, we propose in this chapter a mechanism, based on a paper of Gurevich et al [3]. In this paper the transport coefficients are given in terms of the correlation function of the pertirbations of the magnetic field.

Gurevich et al [3] first described the motion of the electrons and ions in a magnetic field, writing their kinetic equations in the drift approximation. This is presented in the section (4.2). As the analysis of the kinetic equation for real systems is very complicated, they calculated the moments of this equation, obtaining the hydrodynamic equations for the plasma number density, the average velocity, the current and the electron and ions temperatures. In these hydrodynamic equations, the transport coefficients appear in terms of the correlation function $F(b_r)$ of the perturbations of the magnetic field. This is presented in the

section (4.3). It is possible to check the accuracy of the description of the RFP configuration with these hydrodynamic equations, comparing their results with the data obtained in the experiments. In the experiences, after an initial transient process, a quasisteady state is achieved. The data obtained in this state can be compared with the ones of the hydrodynamic equations, if we apply on these the condition that the system is stationary. This is done in section (4.4), and it is possible to see that the agreement between the data is very good.

The mechanism we propose to account for the effect of the perturbative magnetic field on the time evolution of the magnetuc profile is the following: given a certain initial magnetic profile $B^{(0)}$, we evolve the system until a time $t^{(1)} = t^{(0)} + \Delta t$. At this time, we see the perturbative spectrum that appears, $b^{(1)}$, add to the initial profile $B^{(1)} = B^{(0)} + b^{(1)}$ and calculate the correlation function $F(b^{(1)})$. We evolve again the system until a time $t^{(2)} = t^{(1)} + \Delta t$, considering as starting values $B^{(1)}$ and $F(B^{(1)})$. At $t^{(2)}$ we again analyse the perturbative spectrum $b^{(2)}$ and calculate $B^{(2)} = B^{(1)} + b^{(2)}$ and $F(b^{(2)})$. The processs is repeated until the saturation of the modes. This is presented in section (4.5).

4.2 The Kinetic equation

We consider that the plasma is in a magnetic field $\mathbf{B}$, consisting of regular and fluctuating components, $\mathbf{B}_0$ and $\mathbf{b}$[3]:

$$\mathbf{B} = \mathbf{B}_0 + \mathbf{b} \tag{4.1}$$

$$|\mathbf{b}| << |\mathbf{B}_0| \tag{4.2}$$

The basic quantities characterizing these fluctuations are the correlations length L_c and correlation time τ_c. These quantities are considered large in comparison with the gyroradii and the inverse gyrofrequencies of the ions and electrons. So it is possible to describe the motion of the electrons and ions in the drift approximation:

$$\Delta f = S(f) \tag{4.3}$$

where Δ is an operator:

$$\Delta \equiv \frac{\partial}{\partial t} + \mathbf{V}\frac{\partial}{\partial \mathbf{r}} + \frac{\partial u}{\partial t}\frac{\partial}{\partial u} + \frac{\partial \mu}{\partial t}\frac{\partial}{\partial \mu}, \tag{4.4}$$

$f = f(u, \mu, \mathbf{r}, t)$ is the particle distribution function, $\mathbf{V}$ is the particle velocity, given by the sum of u, the velocity along the magnetic field, and $\mathbf{V}_{drift}$, the drift velocity. $S(f)$ is the collision integral and μ is the adiabatic invariant. The drift approximation and the drift velocity are presented in the appendix D.

Considering that the magnetic field consists of two parts, one regular and another fluctuating, it is also possible to write the distribution function in these terms. One regular part, f_0, that is an average over the fluctuating parts, and δf, a fluctuating part:

$$f = f_0 + \delta f \tag{4.5}$$

where $|\delta f| << |f_0|$.

The kinetic equation becomes:

$$(\Delta_0 + \Delta_1)(f_0 + \delta f) = S(f_0 + \delta f) \tag{4.6}$$

where

$$\Delta_0 \equiv \frac{\partial}{\partial t} + \mathbf{V}_0\frac{\partial}{\partial \mathbf{r}} + (\frac{\partial u}{\partial t})_0\frac{\partial}{\partial u} + (\frac{\partial \mu}{\partial t})_0\frac{\partial}{\partial \mu} \tag{4.7}$$

and

$$\Delta_1 \equiv \delta\mathbf{V}\frac{\partial}{\partial \mathbf{r}} + \delta(\frac{\partial u}{\partial t})\frac{\partial}{\partial u} + \delta(\frac{\partial \mu}{\partial t})\frac{\partial}{\partial \mu}. \tag{4.8}$$

In these equation it is considered that all quantities can be written as regular and fluctuating part. The quantities δv, $\delta(\frac{du}{dt})$ and$\delta(\frac{d\mu}{dt})$ are linear in the b/B_0 corrections and the operator Δ_1 is given explictly by:

$$\Delta_1 = u\frac{b_r}{B_0}\frac{\partial}{\partial r} + (\frac{e}{m}\frac{E_r}{B} - \frac{\mu}{2}\frac{1}{B}\frac{\partial B}{\partial r})b_r\frac{\partial}{\partial u} \tag{4.9}$$

Averaging the equation (4.6) over an ensemble of random values $\mathbf{b}$, we obtain:

$$\Delta_0 f_0 + < \Delta_1 \delta f > = < S(f_0 + \delta f) > . \tag{4.10}$$

This equation describes the time evolution of the averaged distribuition function. But this equation contains the fluctuating term

δf. So, it is necessary to solve the kinetic equation to the fluctuating part in order to have a complete description of the motion of the averaged term. The kinetic equation is obtained subtracting the average kinetic equation (4.10) from the toroidal kinetic equation (4.6):

$$\Delta_0 \delta f = -\Delta_1 f_0 + [S(f_0 + \delta f) - < S(f_0 + \delta f) >] - [\Delta_1 \delta f - < \Delta_1 \delta f >] \quad (4.11)$$

In order to solve this equation two aproximations are done. One is to neglect the collisions terms. It is possible to do this approximation because in the cases of interest the ion and electron mean free path are considerably longer than the longitudinal (parallel to the magnetic field) correlation length. Another approximation is to consider just the leading term of the expression $[\Delta_1 \delta f - < \Delta_1 \delta f >]$ that is given by

$$[\Delta_1 \delta f - < \Delta_1 \delta f >] = u \frac{br}{B_0} \frac{\partial}{\partial r}. \quad (4.12)$$

With these approximations, we have:

$$\Delta_0 \delta f + u \frac{b_r}{B_0} \frac{\partial}{\partial r} \delta f = -\Delta_1 f_0. \quad (4.13)$$

Solving this equation we obtain for δf:

$$\delta f = \int_0^\infty d\tau \int_{-\infty}^\infty G(\tau/\tau') \Delta_1' f_0' d\tau' \quad (4.14)$$

where $G(\tau/\tau')$ is the Green's function for equation (4.13) and τ is the phase-space volume. In cylindrical geometry, and considering that the particles follow the magnetic lines, the Green's function is given by:

$$G(\tau/\tau') = \Theta(\tau)\delta(\theta - \theta' - \frac{h_\theta}{r} u\tau)\delta(z - z' - h_z u\tau) \delta(r - r' - \frac{b^{m,n}(r^*_{m,n})}{B} \Delta_{m,n} u\tau)\delta(u - u')\delta(\mu - \mu') \quad (4.15)$$

where $b^{m,n}$ are the Fourier components of the magnetic fluctuations b_r, $r^*_{m,n}$ is the radius of the resonant surface, defined by the condition

$$\frac{m}{r^*_{m,n}} B_\theta(r^*_{m,n}) + \frac{n}{R} B_z(r^*_{m,n}) = 0 \tag{4.16}$$

and $\Delta_{m,n}$ is a number that is equal to unity if $r = r^*_{m,n}$ and vanishes otherwise.

Assuming that the function f (from here we will call f_0 just f) is independent of z and θ and that the magnetic field fluctuations b are homogeneous and isotropic in θ, z, and t, we finally get the following equation:

$$\frac{\partial f}{\partial t} + < V_{drift} > \frac{\partial f}{\partial r} + < \frac{du}{dt} > \frac{\partial f}{\partial u} = I(f) + St(f) \tag{4.17}$$

where

$$I(f) = \frac{u}{B}\frac{1}{r}\frac{\partial}{\partial r}[rK] + \frac{\partial}{\partial u}[(\frac{e}{E}\frac{E_r}{B} - \frac{\mu}{2}\frac{1}{B}\frac{\partial b}{\partial r})K] \tag{4.18}$$

$$K = \frac{u}{B}\frac{F}{|u|}\frac{\partial f}{\partial r} + \frac{\partial f}{\partial u}[\frac{eE_r}{mB} - \frac{\mu}{2B}\frac{\partial B}{\partial r})]\frac{f}{|u|}] \tag{4.19}$$

$$F = \int_0^\infty dL < b_r b'_r >, dL = |u| d\tau \tag{4.20}$$

$$b'_r = b_r(\theta - \frac{h_\theta L}{r}, z - h_z L, r - \frac{b^{m,n}(r^*)}{B}\Delta_{m,n} L) \tag{4.21}$$

The kinetic equation (4.17) shows that in cylindrical geometry the plasma dynamics is described by a single correlation function $F(r)$, which is determined by the fluctuations b_r of the magnetic field.

4.3 Hydrodynamic Equations

Analysis of the kinetic equation (4.17) for real systems is extremely complicated. It is therefore natural to go over to a hydrodynamic description of the plasma. This is valid if the plasma variables do not change significantly over an electron collision time:

$$\frac{dT_e}{dt} < \nu_{ei} T_e \tag{4.22}$$

$$\frac{du}{dt} < \nu_{ei} u \tag{4.23}$$

where ν_{ei} is the electron collision frequency and T_e and u are the electron temperature and hydrodynamic velocity.

Substituing the Maxwell distribution function in (4.17) and introducing the hydrodynamic velocity

$$V_p = (\frac{m_e u_e + m_i u_i}{m_e + m_i}) \tag{4.24}$$

and the electric current $J = ne(u_i - u_e)$ parallel to the magnetic field, after taking moments we arrive at the following system of hydrodynamics equations for the plasma number density n, the average velocity V_p, the current J_p, and the electron and ion temperatures T_e and T_i:

$$\frac{\partial n}{\partial t} + \frac{1}{r}\frac{\partial}{\partial r}(rnV_{drift}) = \frac{1}{r}\frac{\partial}{\partial r} r[D_1 \frac{\partial n}{\partial r} + D_2 \frac{\partial T_e}{\partial r} + D_3 \frac{\partial T_i}{\partial r}] + Q_n \tag{4.25}$$

$$\frac{\partial J_p}{\partial t} + \frac{1}{r}\frac{\partial}{\partial r}(rV_{drift}J_p) = \frac{1}{r}\frac{\partial}{\partial r}(rR_1) + R_2 - \nu_{e,i}J_p + \frac{e^2 n}{m_c}E_p \tag{4.26}$$

$$\frac{\partial}{\partial t}(V_p n) + \frac{1}{r}\frac{\partial}{\partial r}(rnV_{drift}V_p) = \frac{1}{r}\frac{\partial}{\partial r}(r\Pi_1) + \Pi_2 \tag{4.27}$$

$$\frac{3}{2}\frac{\partial}{\partial t}(nT_e) + \frac{3}{2}\frac{1}{r}\frac{\partial}{\partial r}(rV_{drift}nT_e) = \frac{2}{r}\frac{\partial}{\partial r} r[T_e J_d + \frac{F}{\pi^{1/2}B^2}(\frac{2T_e}{m_e})^{1/2} n \frac{\partial T_e}{\partial r}] + 2eE_r J_d + J_p E_p + \frac{1}{r}\frac{\partial}{\partial r}(r\chi_L^e \frac{\partial T_e}{\partial r}) + Q_e \tag{4.28}$$

$$\frac{3}{2}\frac{\partial}{\partial t}(nT_i) + \frac{3}{2}\frac{1}{r}\frac{\partial}{\partial r}(rV_{drift}nT_i) = \frac{2}{r}\frac{\partial}{\partial r}[T_i J_d + \frac{F}{\pi^{1/2}B^2}(\frac{2T_i}{m_i})^{1/2} n \frac{\partial T_i}{\partial r}] + 2eE_r J_d + \frac{1}{r}\frac{\partial}{\partial r}(r\chi_L^i \frac{\partial T_i}{\partial r}) + Q_i \tag{4.29}$$

where

$$J_d = D_1 \frac{\partial n}{\partial r} + D_2 \frac{\partial T_e}{\partial r} + D_3 \frac{\partial T_i}{\partial r} \tag{4.30}$$

and the coefficients D_1, D_2 and D_3 are defined by the relations:

$$D_1 = \frac{D_i D_e (T_e + T_i)}{D_e T_i + D_i + T_e} \tag{4.31}$$

$$D_2 = \frac{D_e^T D_i T_e}{D_e T_i + D_i + T_e} \tag{4.32}$$

$$D_3 = \frac{D_i^T D_e T_i}{D_e T_i + D_i + T_e} \tag{4.33}$$

$$D_{i,e} = \frac{F}{\pi^{1/2} B^2} \left(\frac{2T_{i,e}}{m_{i,e}}\right)^{1/2} + D_{i,e}^{cl} \tag{4.34}$$

$$D_{i,e}^T = \frac{F}{\pi^{1/2} B^2} \frac{n}{2T_{i,e}} \left(\frac{2T_{i,e}}{m_{i,e}}\right)^{1/2} \tag{4.35}$$

$D_{i,e}^{cl}$ and $D_{i,e}^{Tcl}$ are the classical particle and thermal diffusivities respectively and $\chi_L^{i,e}$ are the classical transverse ion and electron thermal conductivities.

The expressions R_1 and Π_1 result from electron and ion scattering by fluctuations. This scattering gives rise to current and velocity diffusion:

$$R_1 = \frac{F}{\pi^{1/2} B^2} \{2 \left(\frac{2T_e}{m_e}\right)^{1/2} \frac{\partial J_p}{\partial r} + \frac{2e}{m_e} E_r \left(\frac{m_e}{2T_e}\right)^{1/2} + \frac{J_p}{B} \frac{\partial B}{\partial r} \left(\frac{2T_e}{m_e}\right)^{1/2} J_p\} \tag{4.36}$$

$$\Pi_1 = \frac{F}{\pi^{1/2} B^2} \{2 \frac{\partial}{\partial r} [n \left(\frac{2T_i}{m_i}\right)^{1/2} V_p] - \frac{2e}{m_i} E_r n V_p \left(\frac{m_i}{2T_i}\right)^{1/2} - \frac{1}{B} \frac{\partial}{\partial r} B \left(\frac{2T_i}{m_i}\right)^{1/2} n V_p\} \tag{4.37}$$

A frictional force also arises as a result of the interaction between the charged particles and the fluctuations. It is described by the terms R_2 for the electrons and Π_2 for the ions:

$$R_2 = \frac{F}{\pi^{1/2}B^2}\{\frac{2e}{m_e}E_r\frac{\partial}{\partial r}[(\frac{m_e}{2T_e})^{1/2}J_p] + \frac{1}{B}\frac{\partial B}{\partial r}\frac{\partial}{\partial r}[(\frac{2T_e}{m_e})^{1/2}J_p] + 4(\frac{e}{m_e}E_r)^2(\frac{m_e}{2T_e})^{3/2}J_p + \frac{4e}{m_e}E_r\frac{\partial B}{\partial r}\frac{1}{B}(\frac{m_e}{2T_e})^{1/2}J_p + \frac{3}{2}(\frac{1}{B}\frac{\partial B}{\partial r})^2(\frac{m_e}{2T_e})^{-1/2}J_p \quad (4.38)$$

$$\Pi_2 = -\frac{F}{\pi^{1/2}B^2}\{\frac{2e}{m_i}E_r\frac{\partial}{\partial r}[(\frac{m_e}{2T_e})^{1/2}nV_p] - \frac{1}{B}\frac{\partial B}{\partial r}\frac{\partial}{\partial r}[(\frac{2T_i}{m_i})^{1/2}nV_p] - 4(\frac{e}{m_i}E_r)^2(\frac{m_i}{2T_i})^{3/2}nV_p + \frac{4e}{m_i}E_r\frac{\partial B}{\partial r}\frac{1}{B}(\frac{m_i}{2T_i})^{1/2}nV_p - \frac{3}{2}(\frac{1}{B}\frac{\partial B}{\partial r})^2(\frac{m_i}{2T_i})^{-1/2}nV_p \quad (4.39)$$

The equations describing heat and particle transport include external heat sources Q_e, Q_i and an ionization rate Q_n. These equations must be suplemented by the Maxwell equations. We can see that in these equations the effect of the perturbation of the magnetic field on the transport coefficients is considered. These coefficients are functions of the correlation function $F(b_r)$ of the magnetic perturbations.

4.4 Stationary State

One characteristic of the dynamics of a toroidal pinch experiment is that after an initial highly turbulent phase, the plasma settles into a more quiescent state, where the current and the magnetic field change smoothly during the lifetime of the discharge. This process can be considered stationary.

Considering the case that $\beta << 1$ ($\mathbf{J}//\mathbf{B}$), we obtain for the magnetic field $\mathbf{B}$ and the current J_p in the stationary state the following equations:

$$\mathrm{L}J_p = 0 \tag{4.40}$$

$$\nabla \times \mathrm{B} = \frac{4\pi}{c} J_p \mathrm{h} \tag{4.41}$$

$$\nabla.\mathrm{B} = 0 \tag{4.42}$$

where the differential operator L is defined by the following expression:

$$\mathrm{L}J_p = \frac{1}{r}\frac{\partial}{\partial r}(rR_1) + R_2 \tag{4.43}$$

In this operator the term which describes the classical collisional resistivity has been neglected because at sufficiently high temperatures it is small compared with the resistivity due to fluctuations. The equations (4.42) are solved numerically by iteration for a given correlation function $F(r)$.

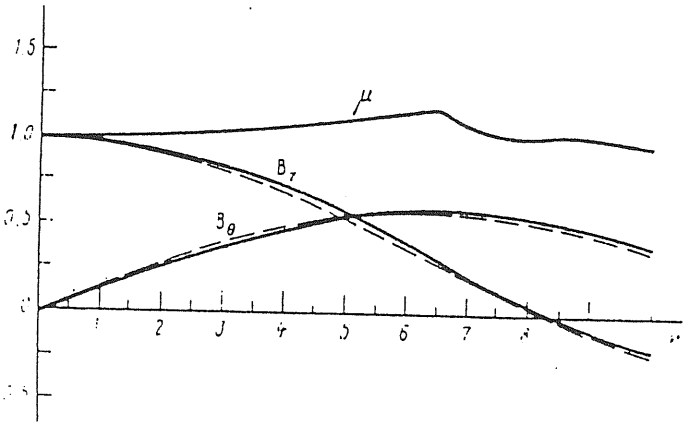

Figure 4.1: $B_\theta(r)$, $B_z(r)$ and $\mu(r)$ obtained for the stationary state, when the density and temperature are considered constants. The broken trace is the result of the Taylor theory. (Figure taken from the reference [3].)

Considering that n=constant and T=constant, the magnetic profiles obtained from the equations (4.42) are very similar to the ones given by the Taylor theory of the relaxed states. On the other hand, the quantity $\mu = J_p/B$ is not uniform as the Taylor theory assumes. It is almost uniform until a certain value of r and then it diminishes close to $r = a$. This result agrees with the experimental observations. The profiles $B_z(r)$, $B_\theta(r)$ and $\mu(r)$ can be seen in the figure (4.1).

The magnetic profiles can be characterized by two parameters, the F and Θ parameters, that are given by:

$$F = \frac{B_z(r=a)}{< B_z >} \tag{4.44}$$

$$\Theta = \frac{B_\theta(r=a)}{< B_z >} \tag{4.45}$$

with these parameters we can compose the $F-\Theta$ diagram. Considering n=constant and T=constant, the $F-\Theta$ diagram that is obtained is very similar to the one associated with Taylor theory, as can be seen in the figure (4.2).

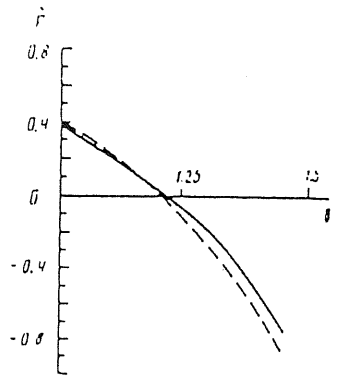

Figure 4.2: $F - \Theta$ diagram describing the stationary states, when the density and temperature are considered constants. The broken trace is the result of the Taylor theory. (Figure taken from the reference [3].)

If, instead of considering the density and temperature constants, one uses the following profiles:

$$\frac{n}{n_0} = 1 - (\frac{r}{a})^2 \tag{4.46}$$

and

$$\frac{T_e}{T_0} = 1 - (\frac{r}{a})^4, \tag{4.47}$$

the magnetic profiles obtained are almost the same as before. But, the quantity μ undergoes a substantial modification, as can be seen in the figure (4.3). The diagram $F - \Theta$ also changed very much, with values that agree satisfactory with experimental data, as shows the figure (4.4).

Thus the solution of equations (4.40)-(4.42) provides a good description of the existence and properties of the relaxed state in an RFP configuration.

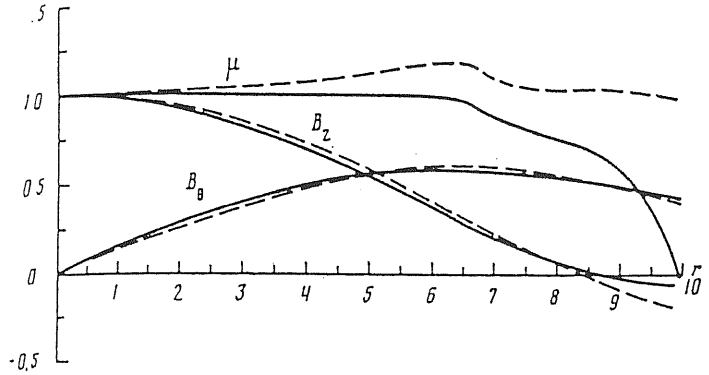

Figure 4.3: $B_\theta(r)$, $B_z(r)$ and $\mu(r)$ obtained for the stationary state, when the density and temperature have the profile given by the equations (3.46) and (3.47) respectively. The broken trace is the result for the stationary state, when the density and temperature are contants. (Figure taken from the reference [3].)

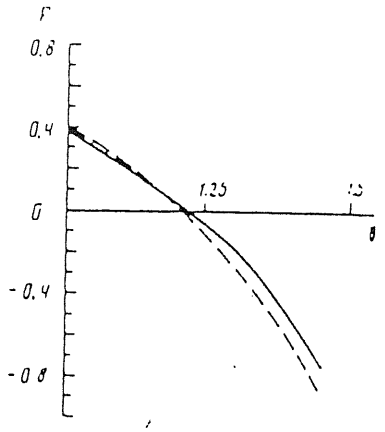

Figure 4.4: $F - \Theta$ diagram for the stationary state, when the density and temperature profile are given by the equations (3.46) and (3.47) respectively. The broken trace is the result for n=constant, T=constant and the dot-dash trace is the Taylor's solution. The points are experimental results. (Figure taken from the reference [3].)

4.5 Self-Consistent Approach

We can account for the effect of the perturbations of the magnetic field on the time evolution of the equations of the magnetic field lines througth the transport coefficients. These coefficients are written in terms of the correlation function of these perturbations:

$$F(r) = \int_0^\infty d\tau < b_r b'_r >, \tag{4.48}$$

as it was shown in the preceding sections.

To have a closed system we have to be able to calculate $F(r)$.

In order to calculate $F(r)$, we must know the fluctuations modes that exist in the system. This can be done writing the time evolution equations to the fluctuations u and b, that are obtained subtracting the equations of the stationary state from the hydrodynamic equations. They are given by:

$$\frac{\partial \mathrm{u}}{\partial t} + (\mathrm{u}\nabla)\mathrm{u} = \frac{1}{4\pi m_i n}\{[\mathrm{B} \times (\nabla \times \mathrm{b})] + [\mathrm{b} \times (\nabla \times \mathrm{B})] +$$

$$[\mathbf{b} \times (\nabla \times \mathbf{b})]\} + \frac{\mathbf{B}}{Bn}\{\frac{1}{r}\frac{\partial}{\partial r}(r\Pi_1) + \Pi_2\} \quad (4.49)$$

$$\frac{\partial \mathbf{b}}{\partial t} = \nabla \times [\mathbf{u} \times (\mathbf{B} + \mathbf{b})] +$$
$$\nabla \times \{\frac{\mathbf{b}}{B}\frac{m_e}{4\pi e^2 n}\mathbf{L}(\frac{\mathbf{B}}{B}.\nabla \times \mathbf{b})\} + \eta_m \Delta \mathbf{b} \quad (4.50)$$

$$\nabla.\mathbf{b} = 0 \quad (4.51)$$

Taking a certain magnetic profile $B^{(0)}$, we can use the equations (4.49), (4.50) and (4.51) to calculate the perturbative modes that will appear in this system. After a certain time interval Δt, we take the modes that growed, $b^{(1)}$, add to the initial profile $B^{(0)} + b^{(1)} = B^{(1)}$ and calculate the correlation function of this perturbation, $F(b^{(1)})$. Taking the values of $B^{(1)}$ and $F(b^{(1)})$ as initial configuration at time step $t^{(1)} = t^{(0)} + \Delta t$, evolving again the system until time $t^{(2)} = t^{(1)} + \Delta t$, we take the values of the modes $b^{(2)}$, add to the preceding profile, $B^{(2)} = B^{(1)} + b^{(2)}$ and compute $F(b^{(2)})$. The process continues until the saturation of the modes. In the proposed process the effect of the perturbations of the magnetic field is up-dated at each time interval, when the correlation function $F(b)$ is calculated.

Appendix A

Expressions and Parameters

The spectra of the perturbative cxomponent of the magnetic field $\mathbf{B}^{(1)}$ are given by experimental observations. The main modes of the poloidal serie are $m = 0, 1$. The toroidal spectrum is essencially concentrated in the range $7 \leq n \leq 18$ peaked around $n = 8$.

The Poincaré map in $\theta = 2\pi$ for the equation of motion (2.34) is given by:

$$\begin{cases} \rho_{k+1} &= \rho_k + \epsilon F(\rho_{k+1}, \psi_k) \\ \psi_{k+1} &= \psi_k + \omega(\rho_{k+1}) + \epsilon G(\rho_k, \psi_k) \end{cases} \tag{A.1}$$

where

$$\begin{aligned} F(\psi, \theta) &= \frac{2}{\mu} \frac{2\rho(a - \rho^{1/2})}{a^2} \sum_n a_n [b_0 \frac{cos(n\psi) - cos(2\pi n w(\rho) + k\psi)}{n w(\psi)} \\ &+ b_1 \frac{cos(n\psi) - cos(2\pi n w(\rho) + n\psi)}{1 - (n w(\rho))^2}] \end{aligned} \tag{A.2}$$

and

$$\begin{aligned} G(\psi,\theta) &= \textstyle\sum_n a_n[\frac{1}{n}\frac{3\rho^{1/2}-2a)}{a^2}[b_0\frac{sin(2\pi nw(\rho)+n\psi)-sin(n\psi)}{nw(\rho)} \\ &+b_1\frac{cos(n\psi)-cos(2\pi nw(\rho)+n\psi)}{1-(nw(\rho))^2}]+w'(\rho)\frac{\rho(a-\rho^{1/2})}{a^2} \\ &[b_0\frac{2\pi nw(\rho)cos(n\psi)-sin(n\psi)-sin(2\pi nw(\rho)+n\psi)}{(nw(\rho))^2} \\ &2b_1nw(\rho)\frac{cos(n\psi)-cos(2\pi nw(\rho))}{(1-nw(\rho))^2}+2\pi b_1\frac{sin(n\psi)}{1-(nw(\rho))^2}]] \end{aligned} \tag{A.3}$$

The spectra taken was:

$$b_0 = 0.5, b_1 = 1.0. \tag{A.4}$$

and

$$a_k = \begin{cases} 0 & n<8, n>18 \\ n/10 & 8\le n\le 10 \\ 20-n/10 & 10<n\le 18 \end{cases} \tag{A.5}$$

The values choosen for the remaining parameters are taken from the ETA-BETA experiment and are:

$$\mu = 2.6 \qquad a = 15cm \qquad R = 75cm \qquad r_* = \frac{2.4}{2.6}a = .923a \tag{A.6}$$

Appendix B

The Generalized Standard Map

The Generalized Standard Map is defined in a torus $\mathbf{M} : \mathbf{T}\times\mathbf{T} \to \mathbf{T}\times\mathbf{T}$:

$$\mathbf{M} : \begin{cases} \rho_{k+1} = & \rho_k + \epsilon V(\psi_k) \\ \psi_{k+1} = & \psi_k + \rho_{k+1} \end{cases} \tag{B.1}$$

and is periodic in both ψ and ρ with unit period. This map can also be defined in a cylinder $\mathbf{M} : \mathbf{R} \times \mathbf{T} \to \mathbf{R} \times \mathbf{T}$, if one doesn't consider the periodicity in ρ. $\mathbf{M}$ is an area-preserving map, since its Jacobian is unity. In particular, when $V(\psi) = sin(\psi)$, this is the Standard or Chirikov-Taylor Map [8].

When the perturbation is null, we have a map T such that:

$$T : \begin{cases} \rho_{k+1} = & \rho_k \\ \psi_{k+1} = & \psi_k + \omega(\rho_{k+1}) \end{cases} \tag{B.2}$$

The iterates of this map are on a curve Γ_ρ and after each iteration each point on it is rotated through an angle $\omega(\rho)$ that is constant along each curve Γ_ρ. Hence, some curves Γ_ρ are rotated through an angle that is commensurate with a whole rotation, and others through an angle incommensurate with a whole rotation. If $x = (\rho, \psi)$ belongs to a curve Γ such that $\omega = 2\pi\frac{m}{n}$, then $T^n x = x$. Thus, each point of Γ is a fixed point of T^n, and the orbit of x consists of n points. We say that this orbit has length n and is called resonant. If the angle $\omega(\rho)$

that corresponds to Γ_ρ is incommensurate with a whole rotation (2π in this case, since we have considered a map mod 2π), then the points $T^n x$ are everywhere dense on Γ_ρ and the orbit is called nonresonant.

So, an unperturbed map generates two kinds of orbits in the Poincaré section. Given a certain initial condition, the orbit generated can be a dense curve or a finite number of points. But if one takes various initial conditions the Poincaré section will be filled with dense curves. When the perturbation is different from zero, the behaviour of the orbits is more complex. There are two theorems that give us some information about these orbits. These are the Poincaré-Birkhoff and KAM theorems.

The Poincaré-Birkhoff theorem [9] is related with the fixed points of a smooth perturbed area-preserving map T_ϵ:

$$T_\epsilon : \begin{cases} \rho_{k+1} = & \rho_k + \epsilon f(\rho_k, \psi_k) \\ \psi_{k+1} = & \psi_k + \omega(\rho_{k+1}) + \epsilon g(\rho_k, \psi_k) \end{cases} \tag{B.3}$$

Let Γ be the curve of the map T formed with the fixed points of T^n. Let'us consider:

$$\omega(\rho) = 2\pi \frac{m}{n} \qquad\qquad \frac{d\omega}{d\rho} \neq 0 \tag{B.4}$$

As we have already said in the above paragraph, after k iterations of T, each point of Γ returns to its initial position. This property of T is not retained for a small perturbation ($T \to T_\epsilon$). The Poincaré-Birkhoff theorem states that, for ϵ small, T_ϵ^k has $2kn$ fixed points close to the curve Γ.

In fact, let us consider two curves that are invariant under T and close to Γ: namely, the curves Γ^+ and Γ^-, with angles of rotation $\omega^+ > \omega > \omega^-$, where ω is the rotation angle of Γ. Thus, the mapping T^k rotates Γ^+ positively and Γ^- negatively, as can be seen in the figure (B.1). This property still holds for T_ϵ^k if ϵ is small enough.

Thus, on each radius ψ =constant, there exists a point $\rho(\psi, \epsilon)$ which moves under T_ϵ^k along the radius:

$$\psi(T_\epsilon^k \rho(\psi, \epsilon)) = \psi \tag{B.5}$$

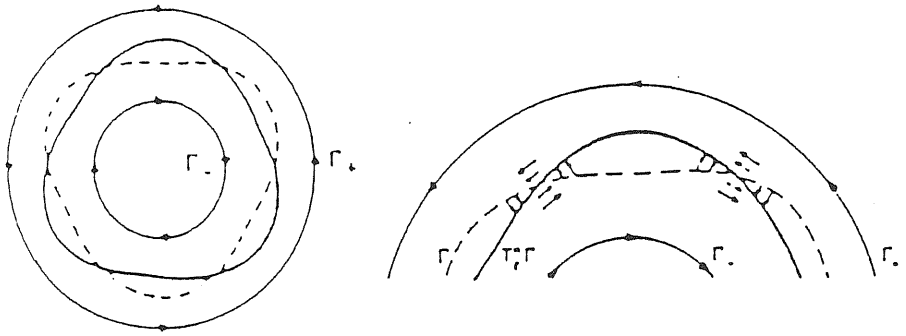

Figure B.1: The mapping T^n rotates Γ^+ positively and Γ^- negatively

Moreover, if ϵ is small enough, the points $r(\psi, \epsilon)$ $(0 \leq \psi \leq 1)$ form a closed analytical curve R_ϵ close to Γ. Now, considering that T_ϵ^k is an area-preserving map, the image $T_\epsilon^k R_\epsilon$ cannot be surrounded by R_ϵ and, conversely, R_ϵ cannot be surrounded by $T_\epsilon^k R_\epsilon$. Thus, R_ϵ and $T_\epsilon^k R_\epsilon$ intersect. The points of intersections are fixed points of T_ϵ^k and the map T_ϵ^k has an even number of fixed points.

The orbits around these fixed points are characterized by their tangent map . One can see that half of the fixed points of T_ϵ^k are elliptic and half hyperbolic and that they alternate themselves.

The iterates of T_ϵ of the points around an elliptic fixed point form ellipses that are called islands, while the iterates T_ϵ of the points around the hyperbolic fixed points move on one or both branches of a hyperbola. So, in this second case, the map T_ϵ takes the points further from the neighborhood of the fixed point.

Given a chain of alternating elliptic and hyperbolic fixed points produced by iterations of T_ϵ, two adjacent hyperbolic fixed point x' and x'' are connected by a trajectory called separatrix. This separatrix encloses the islands that exist around the elliptic fixed point that there is between x' and x''.

It is also interesting to say that inside each island we have the whole system reproduced in a finer scale.

The KAM theorem [9] analyses the behaviour of the orbits associated with an irrational winding number under small perturbation.

Let'us consider a map of the 2n-dimensional "annulus" to itself, which is close to a n-dimensional rotation:

$$\begin{cases} \rho_{k+1} = & r_k + \epsilon f(\rho_k, \psi_k, \epsilon) & r \in B \subset R^n \\ \psi_{k+1} = & \psi_k + \omega(\rho_{k+1}) + \epsilon g(\rho_k, \psi_k, \epsilon) & \psi \mod 2\pi \in T^n \end{cases} \tag{B.6}$$

It is assumed that the map is exact-sympletic, i.e., it preserves the integral of the 1-form $rd\psi$ on closed contours. The unperturbed map ($\epsilon \neq 0$) is said to be nondegenerate if det $(\partial\omega/\partial\rho) \neq 0$.

The KAM theorem formulated to a map states the following: suppose the unperturbed map is analytical and nondegenerate. Then for any small and smooth perturbations, in the 2n-annulus $B \times T^n$ there exist invariant tori close to the tori ρ=constant, and the measure of the complement of their union is small when the perturbation is small. The images of any point of an invariant torus under the iterations of the map densely fill the torus.

Considering a system with only 1 degree of freedom, we obtain an area- preserving map of the ordinary annulus into itself. The restriction of the unperturbed map to each curve ρ=constant is a rotation. The nondegeneracy condition means that the angle of rotation changes from one curve to another. The nonresonant curves that remain distorted under perturbation are those that satisfy the diophantine condition. A winding number ω is called diophantine when $\exists\ \gamma > 0$ and $\exists\ \mu \geq 2$ such that:

$$|\frac{\omega}{2\pi} - \frac{p}{q}|^{-1} < \gamma q^{\mu} \tag{B.7}$$

$\forall\ (p, q) \in \mathbf{Z}$ and $q \neq 0$.

In a perturbed map, like the Generalized Standard Map, the winding number is given by:

$$\omega = \lim_{N\to\infty} \frac{1}{N} \sum_{k=0}^{N} (\psi_{k+1} - \psi_k) \tag{B.8}$$

For these maps, one can observe mainly three kinds of interesting behaviour, as we have already discussed . Two of these exist also for the unperturbed map: the fixed points and the KAM curves, also called zero-dimensional and one-dimensional orbits respectively. The other kind of behaviour are the stochastic regions that appear around the hyperbolic fixed points. These regions are also called two-dimensional orbits.

In the Generalized Standard Map given by equation (B.1), the KAM curves that extend over all the interval $\psi \in [0, 2\pi]$ divide the phase space in disconnected regions. The orbits cannot pass through this KAM curve. So, the KAM curves completely obstruct the diffusion. As the perturbation grows these KAM curves cease to exist, and diffusion is possible.

When all KAM curves that encircle the torus in ψ direction are broken, the map has a behaviour called connected stochasticity. The value of the perturbation parameter at which the last KAM curve is destroyed is called critical.

For values of the perturbation parameter a little higher then the critical one, the destroyed KAM curves are reduced to a cantorian set of points, that affect the diffusion. MacKay, Meiss and Percival [10] have developed a theory of transport that considers this structure of the phase space and have deduced a scale law for the diffusion coefficient near the critical point:

$$D \sim (\epsilon - \epsilon_c)^{\eta} \tag{B.9}$$

This law has been numerically verified [11].

There are some analytical tools to determine the value of the perturbation parameter necessary to destroy a certain KAM curve. The earliest procedure to determine the transition to connected stochasticity was proposed by Chirikov [12] in 1960 and then refined by himself in 1979 [8]. It has been commonly called the Chirikov criterion. In its simplest form, it says that a certain KAM curve is broken when the separatrixes around the elliptic fixed points in opposite sides of the KAM curve touch each other. In this method, the width of the islands around the elliptic fixed points considered are calculated independently. This is one of the reasons why this criterion is neither necessary nor suffi-

cient. If the complete system is solved simultaneously, it may happen that the overlap occurs at another value of the perturbation parameter. And, also, the KAM curve may break before the overlap, due to others factors.

Greene in 1979 [13] has proposed another method, essentially numerical, in which the break of a certain KAM curve is associated with the destabilization of the elliptic fixed points with a rational winding number that approximates the winding number of this KAM curve. This method will be described in more detail in the appendix C.

Following Greene, an invariant curve is approximated by periodic orbits and seems to become non differentiable and self-similar at the critical point, according to Shenker and Kadanoff [14]. A theoretical understanding was then achieved with a renormalization group approach developed by Escande and Doveil in 1981 [15]. This method is based on the analysis of the amplitude of the higher order islands and has been introduced to study the break-up of the invariant curve of the hamiltonian:

$$H(r,\psi,t) = \frac{r^2}{2} - M\cos\psi - P\cos k(\psi - t) \qquad \text{(B.10)}$$

whose Poincaré section, for M=P and k=1 is very similar to the Standard Map.

MacKay in 1983 [16] has extended this procedure to the break-up of an invariant curve with whatever rotation number, introducing an approximate renormalization.

Another method is the use of classical perturbation theory, which proved to be asymptotic in the case of the Birkhoff series [17] and allowed one to determine the boundary of analytically continued invariant curves [18, 19]. Considering the Zehnder [20] formulation of the KAM theorem, this theory can also be applied to describe the behaviour of an invariant curve near the critical point and its break-up mechanism.

Appendix C

The Greene Method

The Greene method [13] is based on an examination of the stability of periodic orbits. It postulates that the disappearance of a KAM curve with an irrational winding number ω is associated with the destabilization of the orbits of the elliptic fixed points with a rational winding number ω' that approximates ω.

An irrational number w can be expressed as a continued fraction expansion:

$$w = \cfrac{1}{a_0 + \cfrac{1}{a_1 + \cfrac{1}{a_2 + \ldots}}} \tag{C.1}$$

where, since $w \leq 1$, the a_n's are positive integers. This is denoted

$$w = [a_0, a_1, a_2, \ldots, a_N] \tag{C.2}$$

which is called the convergent of order N of the irrational w, or w^N. The convergents are unique and as N grows, the approximation is better [21]. The w^N's are rational numbers and the continued fraction expansion is the best way to approximate an irrational with a rational.

Greene has applied his method to find the critical perturbation parameter of the Standard Map. The last KAM curve of this map is expected to be associated with the winding number that most easily

satisfy the diophantine condition. This is given by the winding number associated with the golden mean:

$$w_g = [1,1,1,\ldots] = \frac{\sqrt{5}-1}{2} \tag{C.3}$$

So, it is necessary to analyse the stability of the periodic orbits with winding number given by the convergents of the golden mean. This analysis has been reproduced in my Magister Thesis [22].

Greene found the periodic orbits of the Standard Map using the property that this map can be written as a product of two involutions. When the perturbative spectrum of the Generalized Standard Map **M** is given by a serie in sines, this property is also valid and we have:

$$M = I_2 I_1 \tag{C.4}$$

where

$$I_1 : \begin{cases} \rho_k = & \rho_{k-1} + \epsilon \sum_n a_n \sin(n\theta_{k-1}) \\ \psi_k = & -\psi_{k-1} \end{cases} \tag{C.5}$$

$$I_2 : \begin{cases} \rho_{k+1} = & \rho_k \\ \psi_{k+1} = & -\psi_k + \rho_k \end{cases} \tag{C.6}$$

and

$$I_1^2 = I_2^2 = 1 \tag{C.7}$$

Each of these involutions has lines of fixed points. Namely,

$$I_1(\rho,\psi) = (\rho,\psi) \tag{C.8}$$

is satisfied by $\psi = 0$ or $\psi = \pi$ for any ρ. And

$$I_2(\rho,\psi) = (\rho,\psi) \tag{C.9}$$

is satisfied by $\psi = \pi\rho$ or $\psi = \frac{1}{2}(\rho + 2\pi)$, for any ρ. Some of these fixed points are also fixed points of **M**. The fixed points of **M** of order 2N are those that satisfy the following conditions:

$$I_1(\rho_0,\psi_0) = (\rho_0,\psi_0) \quad and \quad I_2 T^N(\rho_0,\psi_0) = T^N(\rho_0,\psi_0) \tag{C.10}$$

or

$$I_2(\rho_0,\psi_0) = (\rho_0,\psi_0) \quad and \quad I_1 T^N(\rho_0,\psi_0) = T^N(\rho_0,\psi_0) \tag{C.11}$$

while the fixed points of order 2N+1 satisfy:

$$I_1(\rho_0,\psi_0) = (\rho_0,\psi_0) \quad and \quad I_2 T^{N+1}(\rho_0,\psi_0) = T^{N+1}(\rho_0,\psi_0) \tag{C.12}$$

or

$$I_2(\rho_0,\psi_0) = (\rho_0,\psi_0) \quad and \quad I_1 T^N(\rho_0,\psi_0) = T^N(\rho_0,\psi_0) \tag{C.13}$$

Greene says that in this way one finds the fixed points of interest to his method, that are the fixed points that exist until ϵ is very close to zero. In the same way, the KAM curves considered are those that encircle the map, that is, those that exist until ϵ is very close to zero.

The stability of a fixed point can be determined by its tangent space orbit that is obtained linearizing the map. For a set of fixed points of length Q, that is, $T^Q(\rho,\psi) = (\rho,\psi)$, the tangent map is given by

$$\begin{pmatrix} \delta\rho_Q \\ \delta\psi_Q \end{pmatrix} = A \begin{pmatrix} \delta\rho_0 \\ \delta\psi_0 \end{pmatrix} \tag{C.14}$$

where

$$A = \prod_{k=1}^{Q} \begin{pmatrix} \frac{\delta\rho_{k+1}}{\delta\rho_k} & \frac{\delta\rho_{k+1}}{\delta\psi_k} \\ \frac{\delta\psi_{k+1}}{\delta\rho_k} & \frac{\delta\psi_{k+1}}{\delta\psi_k} \end{pmatrix} \tag{C.15}$$

If $|TrA| > 2$ the fixed points are hyperbolic (unstable) and if $|TrA| < 2$ they are elliptic (stable).

Greene defines a quantity called residue [23]:

$$R = \frac{1}{4}(2 - TrA) \tag{C.16}$$

According to the results above, when $0 < R < 1$ the fixed points are elliptic and when $R < 0$ or $R > 1$, they are hyperbolic.

According to Bountis and Helleman [24, 25] this residue can also be written as the determinant of a $Q \times Q$ matrix:

$$R = -\frac{1}{4} DetH. \tag{C.17}$$

For the Standard Map the matrix H is given by:

$$H = \begin{pmatrix} 2+\epsilon\cos\psi_1 & -1 & \dots & -1 \\ -1 & 2+\epsilon\cos\psi_2 & & \\ 0 & -1 & & \\ \vdots & & \ddots & \\ -1 & & & 2+\epsilon\cos\psi_Q \end{pmatrix} \tag{C.18}$$

H is tridiagonal with additional -1's in the corners.

It is apparent that when the perturbative parameter ϵ is large, the residue is proportional to ϵ^Q. Greene has shown [13] that this is also true in the limit of small ϵ.

Considering this dependence of the residue on the length of the orbit, Greene has introduced a new quantity, called the mean residue f [13],

$$f \equiv (\frac{|R|}{\beta})^{1/Q}. \tag{C.19}$$

In this way one has a quantity to characterize the break-up of a KAM curve the value of which is independent of the periodic orbit considered. The quantity β can be adjusted for convenience and the mean residue can be evaluated for orbits with negative and positive residues.

Appendix D

The Drift Approximation

The basic quantities characterizing the magnetic fluctuations are the correlations length L_c and correlation time τ_c. These quantities are considered large in comparison with the gyroradii and the inverse gyrofrequencies of the ions and electrons.

The gyroradius and gyrofrequency of a charged particle is determined by its motion in a constant and uniform magnetic field. The trajectory is a helix with its axis parallel (or anti-parallel) to $\mathbf{B}$, or we can say that it is the motion of a particle along the magnetic field, called guiding-center motion, and a rotation around this motion. This motion defines a fundamental frequency, the gyrofrequency w_c, and a fundamental length, the gyroradius r_L.

As we are considering that

$$L_c >> r_L, \tau_c >> w_c^{-1} \tag{D.1}$$

We can describe the motion of the electrons and ions in the drift approximation [45], that considers just the motion of the guiding-center. In this case, the velocity of particle $\mathbf{V}$ is described by the velocity u along the magnetic field and the drift velocity, that is the velocity of a charged particle in an electric and magnetic field. In particular, the drift velocity of a charged particle in a constant and uniform eletric and magnetic field is given by [46]:

$$\mathbf{V}^{(1)}_{drift} = \frac{c^2 \mathbf{E} \times \mathbf{B}}{B^2} \tag{D.2}$$

The drift velocity of a charged particle in a non uniform magnetic field is[46]:

$$\mathbf{V}^{(2)}_{drift} = \frac{mc}{2q}\frac{u_p^2}{B}[\frac{\mathbf{B}}{B} \times \frac{\nabla B}{B}] + (\frac{\mathbf{B}}{B}.\nabla \times \frac{\mathbf{B}}{B})\frac{\mathbf{B}}{B}] \tag{D.3}$$

where u_p is the velocity of rotation around the guiding center. The first term is due to the gradient of $\mathbf{B}$ and the resultant velocity is perpendicular to $\mathbf{B}$. The second term is due to the shear of the magnetic and causes a twisting of the magnetic flux about each other.

Finally, the drift velocity of a charged particle in a magnetic field that has curvature is [46]:

$$\mathbf{V}^{(3)}_{drift} = \frac{mc}{qB}\frac{u_p^2}{B}[\frac{\mathbf{B}}{B} \times (\frac{\mathbf{B}}{B}.\nabla)\frac{\mathbf{B}}{B}] \tag{D.4}$$

So, the kinetic equations that describe the motions of the electrons and the ions are given in the drift approximation by:

$$\frac{\partial f}{\partial t} + \mathbf{V}\frac{\partial f}{\partial \mathbf{r}} + \frac{\partial u}{\partial t}\frac{\partial f}{\partial u} + \frac{\partial \mu}{\partial t}\frac{\partial f}{\partial \mu} = St(f) \tag{D.5}$$

where $f = f(u, \mu, \mathbf{r}, t)$ is the particle distribution function, $\mathbf{V}$ is the particle velocity, $\mathbf{V} = u\frac{\mathbf{B}}{B} + \mathbf{V}_{drift}$, where $\mathbf{V}_{drift} = \mathbf{V}^{(1)}_{drift} + \mathbf{V}^{(2)}_{drift} + \mathbf{V}^{(3)}_{drift}$. $St(f)$ is the collision integral, and μ is the adiabatic invariant given by:

$$\mu = \frac{u_p^2}{B} \tag{D.6}$$

and the time evolution of the velocity u along the magnetic field is given by:

$$\frac{du}{dt} = \frac{q}{mu}\mathbf{E}.\mathbf{V} - \frac{u_p^2}{2Bu}\mathbf{V}.\frac{\partial \mathbf{B}}{\partial r}. \tag{D.7}$$

Bibliography

[1] J.B.Taylor - Rev. Mod. Phys. **53**, 741 (1986)

[2] G.Turchetti, M.Malavasi, S.Siboni, A.Bazzani, C.Pellacani, S.Rimbaldi - IlNuovo Cimento **103B**, 659 (1989)

[3] A.V.Gurevich, K.P.Zybin and A.V.Lukyanov - Sov. Phys. JETP **71**(2), 261 (1990)

[4] J.B.Taylor - Phys. Rev. Lett. **53**, 1139 (1974)

[5] L.Woltjer - Proc. Nath. Acad. Sci. **44**, 489 (1958)

[6] S. Ortolani in "Twenty Years of Plasma Physics", Proocedings of the ICTP Trieste Meeting, edited by McNamana (World Scientific, Philadelphia, Singapure - 1984), pg. 75

[7] J.Cary and R.G.Littlejohn - Ann. of Phys. **151**, 1 (1983)

[8] B.V.Chirikov - Phys. Rep. **52**, 263 (1979)

[9] V.I.Arnold in "Ergodic Problems of Classical Mechanics", W.A.Benjamin, Inc. - New York, Amsterdam, 1968

[10] R.S.MacKay, J.D.Meiss and I.C.Percival - Physica **13D**, 55 (1984)

[11] I.Dana, N.W.Murray and I.C.Percival - Physica **17D**, 63 (1985)

[12] B.V.Chirikov - Plasma Phys. **1**, 253 (1960)

[13] J.M.Greene - J. Math. Phys. **20**, 1183 (1979)

[14] S.J.Shenker and L.P.Kadanoff - J. Stat. Phys. **27**, 631 (1982)

[15] D.F.Escande and D.Doveil - J. Stat. Phys. **26**, 257 (1981)

[16] R.S.MacKay - Physica **7D**, 283 (1983)

[17] G.Servizi, G.Turchetti, G.Benettin and a.Giorgilli - Phys. lett. **95A**, 11 (1983)

[18] J.M.Greene and I.C.Percival - Physica **3D**, 530 (1981)

[19] I.C.Percival - Physica **6D**, 67 (1982)

[20] D.Salamon and E.Zehnder - Comm. Math. Helv. **64**, 84 (1989)

[21] I.Niven "Irrational Numbers" (Mathematical Association of america, Menasha, Wisconsin, 1956)

[22] N. Reggiani - Magister Thesis: "Standard Map: Properties, Transition to Stochasticity and its Application to a Confined Plasma". Thesis presented at October, 1989, a+t the "International School for Advanced Studies", Trieste, Italy.

[23] J.M.Greene - J. Math. Phys. **9**, 760 (1968)

[24] T.Bountis and R.H.G.Helleman - J. Math. Phys.

[25] R.H.G.Helleman in "Statistical Mechanics and Statistical Methods", edited by U.Landman (Plenum, New York, 1977), pg. 343

[26] A. Bazzani, M. Malavasi, N. Reggiani, S. Siboni, G. Turchetti, "Chaotic Transitions and Anomalous Diffusion in a RFP-confined Plasma: Dependence from Spectral Data" in "Nonlinear Phenomena in Physics of Fluids and Plasmas" - Editors: G. Maino, L. Fronzoni, M. Pettini - World Scientific, 1991.

[27] N. Reggiani and M. Malavasi, "Dependence of the Stochasticity Transition on Spectral Data" in "Physics of Alternative Magnetic Confinement Schemes" - Editors: S. Ortolani e E. Sindoni, - Editrici Compositori, Societa' Italiana di Fisica, 1991.

[28] M. Malavasi and N. Reggiani, "The Break-up of KAM Curves in a Generalized Standard Map", SISSA preprint 82/91/FM.

[29] A.M.Liapunov - Ann. Math. Studies **17**, Princeton (1047)

[30] G.Benettin, L.Galgani and J.M.Strlcyn - Phys. Rev. **A14**, 2338 (1976)

[31] G.Turchetti and S.Vaienti - "Generalized Dimensions of Strange Sets and Cantorian Approximations", pre-print DFUB 87/20, Universitá di Bologna

[32] D.D.Schnack, D.C.Barnes, Z.Mikic, D.S.Harned, E.J.Caramana, R.A.Nebel - Comp. Phys. Comm. **43**, 17 (1986)

[33] D.D.Schnach, E.J.Caramana, R.A.Nebel - Phys Fluids **28**(1), 321 (1985)

[34] P.Kirby - Comp. Phys. Comm. **47**, 17 (1987)

[35] Y.L.Ho, S.C.Prager - Phys. Fluids B **3**(11), 3099 (1991)

[36] D.D.Schnack, S.Ortolani - Nuclear Fusion **30**, 277 (1990)

[37] S.Cappello, R.Paccagnella - Phys. Fluids B 4(3), 611 (1992)

[38] D.D.Schnack, D.C.Baxterand and E.J.Caramana - J. Comp. Phys. **55**, 485 (1984)

[39] C.Canuto, A.Quarteroni, M.Y.Hussaini and T.A.Zang - "Spectral Methods in Fluid Dynamics" (springer-Verlag)

[40] Mirin - Phys. Fluids bf 29(9), 3018 (1986)

[41] J.P.Freidberg - Rev. Mod. Phys. **54**, 801 (1982)

[42] S.K.Lele - "Compact Finite Difference Scheme with Spectral-like Resolution", to appear in J. Comp. Phys.

[43] H.Eisen, W.Heinrichs and K.Witsch - J. Comp. Phys. **96**, 241 (1991)

[44] J.C.Buell - J. Comp. Phys. **95**, 313 (1991)

[45] R.J.Hastie in "Plasma Physics and Nuclear Fusion Research", edited by R.D.Gill (Academic Press, New York, 1982)

[46] S.R.Seshadri - "Fundamentals of Plasma Physics" (American Elsivier Publihing Company Inc., Amsterdam, 1973)